ANL-7792
Reactor Technology

ARGONNE NATIONAL LABORATORY
9700 South Cass Avenue
Argonne, Illinois 60439

PRESSURE-PULSE PROPAGATION IN TWO-PHASE ONE- AND TWO-COMPONENT MIXTURES

by

R. E. Henry, M. A. Grolmes,
and H. K. Fauske

Reactor Analysis and Safety Division

March 1971

TABLE OF CONTENTS

LIST OF FIGURES

LIST OF TABLES

NOMENCLATURE→

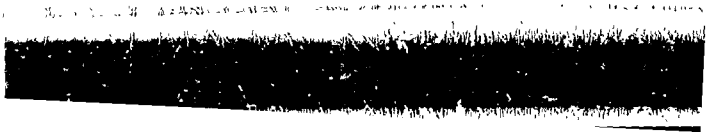

NOMENCLATURE

SYMBOL	DEFINITION
a	propagation velocity of pressure pulse
c	specific heat
C_m	shape or flow parameter for gas bubbles
f	function
k	ratio of vapor to liquid velocity
K	thermal conductivity
L	length of slug-flow element
n	polytropic exponent
P	pressure
q	heat-transfer rate per unit mass
R	gas constant
s	entropy
T	temperature
t	time
u	velocity
v	specific volume
x	vapor mass fraction (quality)
y	dimension normal to interface
z	length (distance)

GREEK LETTERS

α	vapor volume fraction (void fraction)
γ	isentropic exponent - ratio of specific heats for vapor, c_p/c_v
ρ	density
λ	mass-transfer relaxation time

SUBSCRIPTS

a	adiabatic
e	equilibrium
f	saturated liquid
fg	difference between saturated-liquid and vapor properties
g	gas or vapor phase
h	homogeneous
ht	homogeneous isothermal
ha	homogeneous adiabatic
he	homogeneous equilibrium

ℓ
o
p
t
tp
v
SUP
'

ℓ	liquid phase
o	initial condition
p	constant-pressure process for gas phase
t	isothermal
tp	two-phase
v	constant-volume process

SUPERSCRIPTS

′	refers to untransformed coordinate system or frame of reference

PRESSURE-PULSE PROPAGATION IN TWO-PHASE ONE- AND TWO-COMPONENT MIXTURES

by

R. E. Henry, M. A. Grolmes and H. K. Fauske

ABSTRACT

A knowledge of the propagation velocity of pressure pulses in two-phase mixtures has received renewed interest in many areas related to the safety analysis of both water- and liquid-metal-cooled nuclear reactors. A review of the literature has indicated that previous analyses and experiments have been limited to specialized studies of individual flow regimes. No satisfactory analytical and experimental study is available which examines a wide range of dissimilar flow regimes.

In this study a comprehensive analytical development of the propagation velocity of small pressure pulses is presented for bubble, annular, stratified, droplet, and slug-flow regimes. Particular attention is given to the influence of flow regime on the momentum transfer between phases. Momentum transfer in bubbly, droplet, and wavy separated flows is described by consideration of the virtual mass of the discrete phase. For the smooth-interface-separated flows, no interaction is assumed between the phases. In the slug-flow regime, the distinction is made between inertially and acoustically limited pressure propagation, and a consideration of the severe attenuation of a finite pulse on crossing a vapor-liquid interface is shown to be of major importance.

These analyses are compared with data obtained in this and other representative studies. Data obtained in this study are unique in that comparisons of the propagation velocity in one- and two-component mixtures are illustrated for widely different flow regimes. Characteristics of compression and rarefaction pulses in one-component flow are also described. These analyses for small pressure waves satisfactorily explain available data.

I. INTRODUCTION

The phenomena of pressure-pulse propagation in liquid-vapor mixtures is of current interest in the safety analyses for both water-cooled thermal and sodium-cooled fast breeder reactors[1] (LMFBR). For present commercial pressurized and boiling water reactors, two-phase flow in the reactor core occurs normally during steady-state operating conditions. In LMFBR plants, a two-phase system can result from entrainment of cover and fission gases within the coolant and also from coolant boiling following a flow or power transient. Two-phase compressible flow techniques have been proposed to monitor entrained gas levels and to detect coolant boiling and fission gas release. Therefore, a knowledge of two-phase compressible flow behavior will be invaluable in the further development of LMFBR in-core instrumentation as well as in the development of improved analytical models to describe various postulated flow transients.

Previous experimental studies have generally been limited to dispersed flow patterns of bubble and droplet flows. Most theoretical models which have appeared in the literature are homogeneous approaches which are reasonably accurate only for the very low void fractions of bubble flow ($\alpha < 0.20$). A close examination of the equations governing the phenomenon, such as that performed by Fauske,[2] shows that the homogeneous approach does not always adequately describe the phenomenon because such models imply complete momentum transfer between the vapor and liquid phases. This is a result of the assumption of equal vapor and liquid velocity (i.e., velocity ratio $k = 1$). Fauske indicated that the experimental data could be explained by taking into account incomplete momentum transfer between the phases.

It is also significant to note that the homogeneous-bubble-flow regime is not always the most appropriate flow regime in two-phase flow in reactor coolant channels. In water-cooled thermal reactors at high pressures, bubble flow may predominate in normal boiling operation, but for low-pressure LMFBR conditions vapor formation may lead to slug formation.[3,4] Later stages of coolant expulsion may consist of droplet

flow.[5] Various analyses of processes involving expulsion of coolant from channels which assume homogeneous, annular, and slug-type flow regimes have been reviewed by Fauske.[6] Therefore, it seems that all possible flow regimes must be considered in any complete study of the propagation of pressure pulses in two-phase media.

Since there are no measurements of the wave propagation velocity for all flow regimes of interest, the primary objective of this research is to determine experimentally the propagation velocities for various flow configurations. Secondly, the governing equations will be developed, and the various approximations to these relations will be discussed in light of the experimental data of this and other studies. The analytical investigation formulates the interphase momentum-transfer process for the major flow regimes of slug, bubble, droplet, and smooth and wavy interface separated-flow patterns.

II. PREVIOUS WORK

This investigation is primarily concerned with the propagation of a single pulse in a two-phase media. Only the principal studies of this phenomenon to date will be discussed. More extensive discussions of the literature related to the propagation of pressure pulses in two-phase media are to be found in Refs. 7, 8, and 9. In the discussion which follows, previous investigations will be generally categorized by the mixture-flow regime of interest with indications of the salient results of each study.

A. Bubbly Flow

Campbell and Pitcher,[10] along with analysis of shock relations in two-phase homogeneous gas-liquid media, presented experimental results for the propagation velocity of pressure pulses through a mixture of air bubbles in a solution of equal volumes of glycerine and water. The two-phase mixture was produced by passing air through a porous filter at the bottom of a vertical glass test section. The data presented (corrected to 30 in. Hg) for gas volume fractions between 0.05 and 0.30 show good agreement with the well-known homogeneous isothermal expression for the sonic velocity in two-component media (Eq. 26 in this report). The wave speed was measured by recording photocell response to light intensity variations resulting from the different densities in the media as the pressure wave passed two locations a known distance apart. The magnitude of the pressure pulse was varied up to 25 in. Hg with no observed effect on the propagation velocity at a fixed reference pressure and gas volume fraction. It was also noted that compression waves tended to steepen into shock waves while rarefaction waves tended to elongate.

Karplus[11] studied the propagation of strong compression pulses (up to 22-psi amplitude) through a bubbly steam-water mixture to 10 psia. The pulses transmitted through the mixture were of sufficient amplitude to condense the vapor phase completely. The speed of the pulse was measured from the pressure response of two quartz piezoelectric transducers located in the test section a known distance apart. The two-phase

mixture was produced by boiling the water with a wire heater at the base of a vertical test section, producing bubble mixtures with void fractions ranging from 0 to 0.50. Karplus noted the difficulty in defining the speed of the wave because of the failure of compression waves to steepen in his steam-water mixture. Different parts of the pulse were observed to propagate at different velocities, and Karplus determined the velocity associated with the front of the pressure pulse, the pulse at half-height, and the pulse at full amplitude. In general, the measured velocities agreed with the velocity based on a shock model assuming complete condensation behind the passing pressure pulse. It turns out that this model is only superficially different from Eq. 26 discussed later in this report. It is apparent from Karplus' results that compression waves in bubbly steam-water mixtures do not propagate with a speed characteristic of thermodynamic equilibrium.

Semenov and Kosterin[12] measured the velocity of compression pulses in both air-water and steam-water flows of low quality. Their measurements were obtained at somewhat higher pressures of 142, 213, and 285 psia over a range of void fractions from 0.05 to 0.95. Again, measured velocities were in general agreement with the frozen homogeneous model (see Eq. 27). For void fractions between 0.20 and 0.80 the measured velocities were of the order of 100 fps, whereas for void fractions less than 0.20 and greater than 0.80 the measured velocity tended toward the single-phase liquid and vapor velocities, respectively. Semenov and Kosterin also reported better agreement between the measured velocities for air-water mixtures and the frozen homogeneous model than in the case of steam-water mixtures. This point is discussed in Ch. 5.

Walle et al.[13] suggested the use of acoustic methods for the determination of local void fractions in boiling water. They measured the propagation velocity of bursts of high-frequency wave packages in air-water mixtures at 20 psia. The fronts of these bursts were considered equivalent to a single pulse. These measurements were obtained in a somewhat lower gas volume fraction range of 0.001 to 0.1. The results showed a rapid decrease in measured propagation velocity in this void-

fraction region, again in general agreement with the homogeneous propagation model.

DeJong and Firey[14] measured the propagation velocity in liquid-continuous steam-water mixtures at 59, 81, and 99 psia for gas volume fractions less than 0.30. Trends in these measurements were in general agreement with those previously cited;[11] however, several additional interesting observations were made. In such mixtures it was shown that compression and rarefaction waves traveled with the same velocity. The significance of this result relates to the effect of phase change (or lack of effect) on the compressibility of the mixture. Although the amplitude of the pressure pulse was observed to have no significant effect on the propagation velocity, the measured propagation velocity was dependent upon the homogeneity of the mixture. For example, a 25% scatter in the data was reported as a result of variations in the mixture distribution.

The propagation velocities for waves in air-water and steam-water mixtures were also measured by Hamilton.[9] Hamilton's results also showed the velocities characteristic of bubbly mixtures to be in general agreement with predictions of the homogeneous model. His results for strong shock waves, however, show a definite dependency upon the pulse amplitude for void fractions less than 0.10. Two different bubble sizes were used in the air-water study, and the mixture with the larger bubbles exhibited a greater propagation velocity. This was attributed to the difference between isothermal and adiabatic response of the gas. The steam-water data show good agreement between compression and rarefaction waves; however, the velocities appear to be generally less than those reported by previous investigators (see Ch. 5).

The data reported by the above investigators are usually compared to one or both of two homogeneous models. These models are discussed by Hamilton[9] and will be considered in detail in Ch. III. For now it is sufficient to note that these models assume that the general relation for the acoustic velocity in single-phase media:

$$a^2 = -v^2 \frac{dP}{dv} \quad , \tag{1}$$

is valid, the specific volume being written as

$$v = (1 - x)v_\ell + xv_g \quad . \tag{2}$$

In Eq. 2 v is the homogeneous specific volume; hence, the resulting expressions are called homogeneous models. In the evaluation of dv_g/dP, one can assume either an isothermal or an adiabatic path for the derivative. For steam-water mixtures it is usually assumed that the wave passes so rapidly there is insufficient time for mass transfer; hence, the quality, x, is constant or frozen.

Fauske[2] analyzed available data and the governing equation for wave propagation, and demonstrated that the homogeneous models do not completely describe the phenomenon. It was shown that, in addition to describing the interphase heat- and mass-transfer processes, it is also necessary to account for momentum transfer between the constituent phases. The inclusion of this interphase process enabled Fauske to interpret the previously unexplained data of Ref. 12. The importance of momentum transfer was demonstrated, but no mechanism was proposed for the transport.

B. Annular and Droplet Flows

Collingham and Firey[15] measured the propagation speeds for rarefaction waves moving through a one-component, annular-dispersed mixture. The measurements, which were taken at system pressures of 15 and 45 psia and for qualities between 0.10 and 1.0, show the velocities to be essentially equal to the propagation speed in slightly superheated vapor ($\sim$ 1500 fps) and independent of the quality. England et al.[16] refined the above experiment such that only fog (droplet) flows were generated. The results generally agreed with those of Ref. 15; however, a slight decrease was noted with decreasing quality.

DeJong and Firey[14] compared measurements of compression and rarefaction waves in vapor-continuous steam-water mixtures at 45 psia and 50% quality. The results show the velocity of an infinitesimal rarefaction wave to be about 6% less than a compression wave. The compression velocities displayed good agreement with those reported in Ref. 16. Both types of waves showed increasing velocities with increasing wave amplitude in this vapor continuous media.

Evans et al.[7] reported measurements in air-water mixtures for possible flow patterns ranging from slug, to froth, to mist flows. The reported velocities are generally close to 1000 fps; however, a definite decrease was apparent as the local void fraction approached 0.50.

Hamilton[9] also measured the propagation velocities for annular-dispersed air-water flows. His results exhibited good agreement with the single-phase gas sonic velocity.

Garrard[17] reported data for pressure-wave propagation in annularly flowing air-water mixtures. The measured velocities are within 10% of the acoustic velocity of air.

White and D'Arcy[18] reported measurements of propagation velocities for high-pressure, steam-water, annular-dispersed systems. The data were taken at pressures of 485 and 1000 psia, and exhibited the same general characteristics as the low-pressure results of Refs. 7, 9, and 14-17, i.e., the velocities were approximately equal to the single-phase vapor value.

Fauske[2] presented a model for annular- and droplet-flow patterns. In the model no heat or mass transfer occurs and the liquid velocity remains constant. This approach gave good agreement with the high-quality experimental results of Refs. 15 and 16.

However, it is evident from this brief discussion of previous studies that the flow pattern is a distinct means of classifying the phenomenon, and that a systematic investigation and classification of

propagation velocities is needed. The analytical and experimental portions of this study will investigate the compressibility of bubbly, droplet, separated (with both smooth and wavy interfaces), and slug-flow regimes. These simple patterns illustrate the relationship between the flow configuration and the propagation velocity, and they also yield reasonable explanations for the existing data.

III. ANALYSIS

Figure 1 illustrates the one-dimensional propagation of a pressure wave through a stationary gas-liquid mixture. If external and viscous forces (wall shear) are neglected, the one-dimensional equation of motion for the two-phase system may be expressed as

$$\frac{\partial}{\partial t}\left[\alpha\rho_g u_g' + (1-\alpha)\rho_\ell u_\ell'\right] + \frac{\partial}{\partial z}\left[\alpha\rho_g u_g'^2 + (1-\alpha)\rho_\ell u_\ell'^2\right] + \frac{\partial P}{\partial z} = 0. \quad (3)$$

The unsteady continuity equation is

$$\frac{\partial}{\partial t}\left[\alpha\rho_g + (1-\alpha)\rho_\ell\right] + \frac{\partial}{\partial z}\left[\alpha\rho_g u_g' + (1-\alpha)\rho_\ell u_\ell'\right] = 0. \quad (4)$$

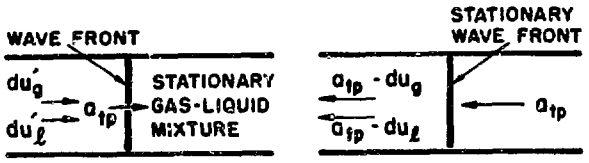

Fig. 1. One-dimensional Model of Wave Propagation

It is assumed in these equations that both the liquid and gaseous phases are present at every cross section of the duct. This is characteristic of the bubbly, stratified, annular, and droplet flow regimes. The slug-flow condition, which does not correspond to this assumption, will be considered later in this chapter. If the coordinate system is transformed from a stationary reference frame to one which travels with the wave, the process is now a steady state, and the momentum and continuity equations can be written as

$$\frac{d}{dz}\left[\alpha\rho_g u_g^2 + (1-\alpha)\rho_\ell u_\ell^2\right] + \frac{dP}{dz} = 0; \quad (5)$$

$$\frac{d}{dz}\left[\alpha\rho_g u_g + (1-\alpha)\rho_\ell u_\ell\right] = 0. \quad (6)$$

When the reference frame is transformed into a Lagrangian system, the stationary gas-liquid mixture is transformed into a two-phase mixture where the gaseous and liquid phases are each traveling toward the wave

front at a velocity equal to the two-phase propagation velocity, a_{tp}. Therefore, the mixture on the upstream side of the wave is homogeneous ($k = 1$), that is,

$$u_g = u_\ell = a_{tp}. \tag{7}$$

On the downstream side of the wave, the liquid and gaseous velocities are

$$u_\ell = a_{tp} - du_\ell \tag{8}$$

and

$$u_g = a_{tp} - du_g, \tag{9}$$

respectively, such that the velocity ratio is

$$k = \frac{a_{tp} - du_g}{a_{tp} - du_\ell}. \tag{10}$$

If the wave is one of small amplitude, such that $a_{tp} >> du_g$ and $a_{tp} >> du_\ell$, then the steady-state velocities behind the wave may be approximated by a_{tp}, and Eqs. 5 and 6 can be simplified to

$$\frac{dP}{dz} + a_{tp}^2 \frac{d}{dz}\left[\alpha\rho_g + (1 - \alpha)\rho_\ell\right] + 2a_{tp}\left[\alpha\rho_g \frac{du_g}{dz} + (1 - \alpha)\rho_\ell \frac{du_\ell}{dz}\right] = 0 \tag{11}$$

and

$$a_{tp} \frac{d}{dz}\left[\alpha\rho_g + (1 - \alpha)\rho_\ell\right] + \alpha\rho_g \frac{du_g}{dz} + (1 - \alpha)\rho_\ell \frac{du_\ell}{dz} = 0. \tag{12}$$

If the variables α, ρ_g, and ρ_ℓ are assumed to be of the form $f[P(z)]$ such that $df/dP = (df/dz)/(dP/dz)$, Eqs. 11 and 12 may be combined to give

$$a_{tp}^2 = \frac{dP}{d[\alpha\rho_g + (1 - \alpha)\rho_\ell]} , \tag{13}$$

an expression for the propagation velocity of a pressure wave through a two-phase mixture.

The void fraction is related to the mixture quality, densities, and velocities by

$$\alpha = \frac{x\rho_\ell}{(1 - x)k\rho_g + x\rho_\ell} . \tag{14}$$

Differentiation of Eq. 14 gives

$$\frac{d\alpha}{dP} = \frac{\alpha(1 - \alpha)}{\rho_\ell}\frac{d\rho_\ell}{dP} + \frac{\alpha(1 - \alpha)}{x(1 - x)}\frac{dx}{dP} - \alpha(1 - \alpha)\frac{dk}{dP} - \frac{\alpha(1 - \alpha)}{\rho_g}\frac{d\rho_g}{dP} , \tag{15}$$

where the steady-state velocity ratio has been set equal to unity in accordance with the small-amplitude assumption discussed above. Eq. 13 can be expanded and combined with Eq. 15 to give the following relationship for the propagation velocity:

$$a_{tp}^2 = \left\{ \left[\alpha^2 + \alpha(1 - \alpha)\frac{\rho_\ell}{\rho_g}\right]\frac{d\rho_g}{dP} + \left[(1 - \alpha)^2 + \alpha(1 - \alpha)\frac{\rho_g}{\rho_\ell}\right]\frac{d\rho_\ell}{dP} \right.$$

$$\left. + (\rho_g - \rho_\ell)\frac{\alpha(1 - \alpha)}{x(1 - x)}\frac{dx}{dP} - \alpha(1 - \alpha)(\rho_g - \rho_\ell)\frac{dk}{dP} \right\}^{-1} . \tag{16}$$

The derivatives $d\rho_g/dP$, $d\rho_\ell/dP$, dx/dP, and dk/dP are functions of the interphase rate processes of heat, mass, and momentum transfer. These derivatives will be discussed separately to illustrate what limits or assumptions may be applied to each.

The term $d\rho_g/dP$ is representative of the gaseous compressibility and is generally described by some polytropic process (Pv_g^n = constant).

The exponent n can be bracketed by $n_t \leq n \leq \gamma$, where n_t is the thermal-equilibrium exponent, which is indicative of complete heat transfer, and γ is the isentropic exponent, which results from a negligible rate of interphase heat transfer.

The term $d\rho_\ell/dP$ characterizes the compressibility of the liquid phase and is essentially independent of the interphase processes. Therefore, this derivative can be approximated by the inverse of the square of the liquid propagation velocity, a_ℓ^{-2}.

The term dk/dP is representative of the rate of interphase momentum transfer. It will be shown later in this chapter that the flow-regime dependency of this derivative results in an order-of-magnitude variation in the propagation velocity. However, in order to outline several standard models which have appeared in the literature, it will initially be assumed that the velocity ratio equals unity and is invariant (dk/dP = 0). As a consequence of this assumption, these solutions are designated as Homogeneous Models.

The term dx/dP represents the interphase rate of mass transfer. For two-component flows, such as air-water mixtures, the mass-transfer rate is zero. (The change in the humidity of the gaseous phase has been neglected.) Therefore, the two-component mixture presents the simplest system to investigate. After the two-component homogeneous solutions have been developed and discussed, the mass transfer in one-component mixtures will be considered.

A. Homogeneous Two-component Models

For homogeneous two-component mixtures the above discussion can be summarized as:

a) $$\frac{d\rho_g}{dP} = \frac{\rho_g}{nP} ;$$

b) $\frac{d\rho_\ell}{dP} = \frac{1}{a_\ell^2}$;

c) $\frac{dk}{dP} = 0$;

d) $\frac{dx}{dP} = 0$.

With the above relations Eq. 16 becomes the standard homogeneous formulation

$$a_h^2 = \left\{ \frac{1}{\left[\alpha^2 + \alpha(1-\alpha)\frac{\rho_\ell}{\rho_g}\right] + \left[(1-\alpha)^2 + \alpha(1-\alpha)\frac{\rho_g}{\rho_\ell}\right]\frac{nP}{\rho_g a_\ell^2}} \right\} \frac{nP}{\rho_g} . \quad (17)$$

Two forms of the homogeneous model have been considered in the two-component literature which differ only in the evaluation the exponent n for the term $d\rho_g/dP$. One, which is designated the Homogeneous Isothermal Model, assumes complete heat transfer at all times such that the temperatures of the gas and liquid phases remain equal: $T_g = T_\ell$. Since there are no velocity or temperature differences between the phases, the system entropy remains constant:

$$ds_o = (1 - x)ds_\ell + xds_g = 0. \quad (18)$$

The entropy changes of the phases can be expressed as

$$ds_g = c_p \frac{dT}{T} - \frac{v_g}{T} dp \quad (19)$$

and

$$ds_\ell = c_\ell \frac{dT}{T} \quad (20)$$

where $T = T_g = T_\ell$. The gas phase is assumed to follow some polytropic process and the perfect gas relation such that

$$Pv_g^n = \text{constant} \tag{21}$$

and

$$Pv_g = RT. \tag{22}$$

Differentiating Eqs. 21 and 22, and substituting into Eq. 19 give

$$ds_g = c_p \frac{dT}{T} - \frac{nR}{n-1} \frac{dT}{T}. \tag{23}$$

Combination of Eqs. 23 and 20 with Eq. 18 gives the following relationship for the polytropic exponent:

$$n_t = \frac{(1-x)c_\ell + xc_p}{(1-x)c_\ell + xc_v}. \tag{24}$$

This formulation is the same as that presented by Tangren et al.[19] For very low qualities, the exponent n is very close to unity, hence the isothermal designation.

The other homogeneous model, designated the Homogeneous Adiabatic Model, assumes that the interphase heat-transfer rate is negligible. This assumption implies a nonequilibrium condition at the vapor-liquid interface; however, there is no change in the entropy of the system until the heat-transfer process begins. Therefore, if one assumes that the behavior of this nonequilibrium condition can be approximated by thermodynamic equilibrium relations, the gas phase compresses or expands adiabatically, the liquid remains at constant temperature, and the system entropy does not change. The polytropic exponent for the gas is equal to the isentropic exponent:

$$n_a = {}^{c_p}/_{c_v} = \gamma. \tag{25}$$

Two standard homogeneous models have been outlined for pressure-wave propagation through a two-component, liquid-gas mixture. They are:

Isothermal

$$a_{ht}^2 = \left\{ \frac{1}{\left[\alpha^2 + \alpha(1-\alpha)\frac{\rho_\ell}{\rho_g}\right] + \left[(1-\alpha)^2 + \alpha(1-\alpha)\frac{\rho_g}{\rho_\ell}\right]\frac{n_t P}{\rho_g a_\ell^2}} \right\} \frac{n_t P}{\rho_g}; \tag{26}$$

Adiabatic

$$a_{ha}^2 = \left\{ \frac{1}{\left[\alpha^2 + \alpha(1-\alpha)\frac{\rho_\ell}{\rho_g}\right] + \left[(1-\alpha)^2 + \alpha(1-\alpha)\frac{\rho_g}{\rho_\ell}\right]\frac{\gamma P}{\rho_g a_\ell^2}} \right\} \frac{\gamma P}{\rho_g}. \tag{27}$$

At moderate and low pressures, the liquid compressibility may be neglected for all but the very small void fractions ($\alpha \gtrsim 0.01$). This simplifies Eqs. 26 and 27 to

$$\frac{a_{ht}^2}{a_g^2} = \left\{ \frac{1}{\alpha^2 + \alpha(1-\alpha)\frac{\rho_\ell}{\rho_g}} \right\} \frac{n_t}{\gamma} \tag{28}$$

and

$$\frac{a_{ha}^2}{a_g^2} = \left\{ \frac{1}{\alpha^2 + \alpha(1-\alpha)\frac{\rho_\ell}{\rho_g}} \right\}, \tag{29}$$

respectively, so that

$$\frac{a_{ht}}{a_{ha}} = \sqrt{\frac{n_t}{\gamma}} \,. \tag{30}$$

In the above, a_g is taken to be the isentropic propagation velocity in the gas phase alone.

B. Homogeneous One-component Models

A one-component mixture is a more complex system because of the additional compressibility induced by the change of phase. It has been shown[20] that in the low-quality critical flow of steam-water mixtures the system compressibility is mainly a function of the interphase mass-transfer rate. The one-component propagation models which have appeared in the literature[21,22] have assumed either an equilibrium or negligible mass-transfer rate between the phases.

For the limiting case of a negligible rate of interphase mass transfer, the one-component system exhibits a two-component behavior; hence, Eqs. 26 and 27 characterize the homogeneous solutions for such a system. It should be noted here that, like negligible heat transfer, negligible mass transfer creates a thermodynamic nonequilibrium situation. For a compression wave, the nonequilibrium is at the liquid-vapor interface because the wave generates subcooled liquid and superheated vapor which are each individually stable. A rarefaction wave generates superheated liquid and supersaturated vapor which are both unstable conditions; hence, the nonequilibrium is not localized to the interface. In order to evaluate either Eq. 26 or 27 it is necessary to assume that these nonequilibrium conditions can be approximated by equilibrium thermodynamics. Within the limits of this assumption, the system entropy is invariant because there is no generation of entropy until the mass transfer begins.

If the mass transfer is assumed to follow a thermodynamic equilibrium path, the system entropy will remain constant because there are no velocity, temperature, or free energy gradients:

$$\frac{ds_o}{dP} = \frac{d}{dP}\left[(1 - x)s_f + xs_g\right] = 0 \ , \tag{31}$$

so that

$$\frac{dx}{dP} = -\left[(1 - x)\frac{ds_f}{dP} + x\frac{ds_g}{dP}\right]/s_{fg} \ . \tag{32}$$

For homogeneous systems, where k = 1,

$$\alpha = \frac{xv_g}{(1 - x)v_f + xv_g} \ . \tag{33}$$

Eq. 16 may be rearranged to yield

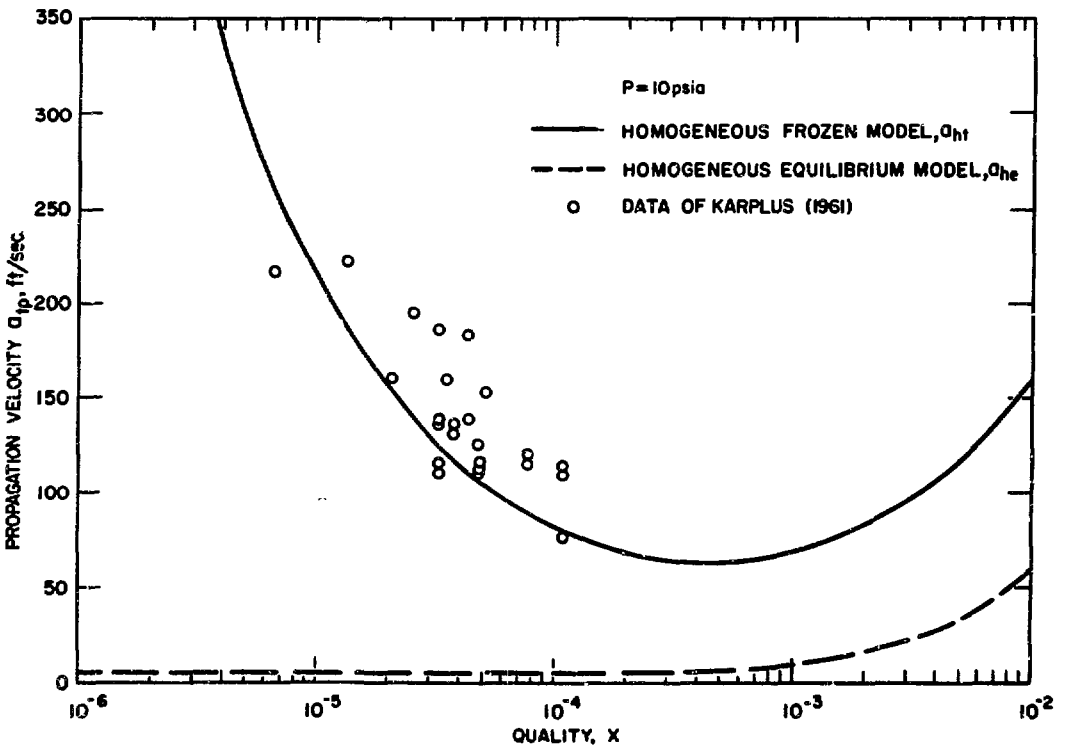

Fig. 2. Comparison of Homogeneous Frozen and Homogeneous Equilibrium Model with Data of Ref. 11 for Pressure-pulse Propagation in Steam-water Mixtures

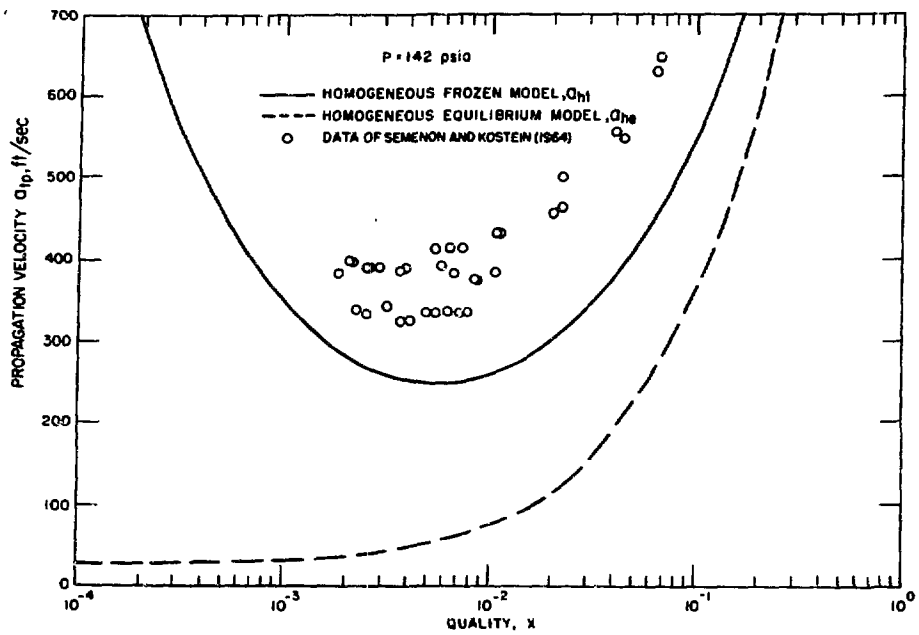

Fig. 3. Comparison of Homogeneous Frozen and Homogeneous Equilibrium Model with Data of Ref. 12 for Pressure-pulse Propagation in Steam-water Mixtures

$$a_h^2 = -\left[(1-x)v_f + xv_g\right]^2 \Big/ \left[x\frac{dv_g}{dP} + (1-x)\frac{dv_f}{dP} + (v_g - v_f)\frac{dx}{dP}\right], \quad (34)$$

which for moderate and low pressures may be simplified to

$$a_h^2 = -\left[(1-x)v_f + xv_g\right]^2 \Big/ \left[x\frac{dv_g}{dP} + v_g\frac{dx}{dP}\right]. \quad (35)$$

Substitution of Eq. 32 into Eq. 35 gives

$$a_{he} = -\left[(1-x)v_f + xv_g\right] \Big/ \left\{x\frac{dv_g}{dP} - v_g\left[\frac{(1-x)\frac{ds_f}{dP} + x\frac{ds_g}{dP}}{s_{fg}}\right]\right\}^{1/2}, \quad (36)$$

where the derivatives dv_g/dP, ds_f/dP, and ds_g/dP can be evaluated from the steam tables. This formulation is entitled the Homogeneous Equilibrium Model.

The Homogeneous Equilibrium and Adiabatic Models for steam-water mixtures are shown in Figs. 2 and 3 for system pressures of 10 and 142

psia, respectively. It is readily apparent that the representation of the mass-transfer process is very critical at low qualities. The experimental steam-water data of Karplus and of Semenov and Kosterin are respectively shown in Figs. 2 and 3. The assumption of negligible rate of mass transfer is more characteristic of the data than the assumption of thermodynamic equilibrium. Therefore, the propagation of an infinitesimal pressure pulse through a stationary, low-quality steam-water mixture essentially exhibits a two-component behavior ($dx/dP = 0$). This result will be compared to the one-component experimental data of this investigation in Ch. 5. Exceptions to this assumption for high-quality flows will be discussed later in this chapter.

Homogeneous frozen and equilibrium models for one-component mixtures have been discussed. A comparison with experimental data shows that $dx/dP = 0$ is a good approximation in the low-quality region. This simplifies Eq. 16 to

$$a_{tp}^2 = \left[\left[\alpha^2 + \alpha(1-\alpha)\frac{\rho_\ell}{\rho_g}\right]\frac{\rho_g}{nP} + \left[(1-\alpha)^2 + \alpha(1-\alpha)\frac{\rho_g}{\rho_\ell}\right]a_\ell^{-2} - \alpha(1-\alpha)(\rho_g - \rho_\ell)\frac{dk}{dP}\right]^{-1} . \tag{37}$$

The experimental studies of Refs. 11 and 12 demonstrate that neither of the two-component homogeneous solutions correctly predict the velocity of wave front propagation. Fauske[2] has numerically analyzed the various interphase rate processes and found that the homogeneous restriction $dk/dP = 0$ is unrealistic. In order to investigate the nature of interphase momentum transfer, it is necessary first to determine a mechanism for interphase momentum transfer; secondly, the dependency upon the flow pattern must be investigated.

The two-phase mixture, which is viewed in the moving reference frame, approaches the wave in an identically homogeneous state, i.e., $u_g = u_\ell = a_{tp}$, and if the wave has an infinitesimal amplitude, the flow on the downstream side is also very nearly homogeneous, as shown by Eq. 10.

Therefore, as the magnitude of the wave becomes small, the relative velocity between the phases approaches zero. This implies that viscous transport is not the principal mechanism for momentum transfer, since such transport is proportional to the relative velocity. However, even though the velocities of the gaseous and liquid phases are nearly equal, the individual accelerations may be quite different. The mechanism can be one which is proportional to the relative acceleration, such as the virtual mass effect associated with a discrete body being accelerated or decelerated with respect to the surrounding fluid. The nature and importance of the virtual mass effect will be investigated for bubbly, droplet, and smooth and wavy interface separated flow patterns.

C. Bubbly Flows

In this section bubbly flow includes all low-quality flows in which the discrete gaseous phase is dispersed throughout the continuous liquid phase. Such flows include gaseous patterns of small isolated spherical bubbles, large interacting nonspherical bubbles, and long bubbly chains.

The momentum equation for a discrete gaseous volume can be expressed[23] as

$$\frac{dP}{dz} = \rho_g u_g \frac{du_g}{dz} + \frac{\rho_\ell}{C_m}\left(u_g \frac{du_g}{dz} - u_\ell \frac{du_\ell}{dz}\right) , \tag{38}$$

where C_m* is a function of the shape of the gaseous volume. If the gaseous phase were in the shape of a spherical bubble, C_m would equal 2. Since the gaseous geometry continually changes as the void fraction increases from 0 to 0.50, the value of C_m may also change. The flow patterns for these low-quality dispersed flows appear to be a strong function of the void fraction; thus, as a first approximation, it seems reasonable to assume C_m is only a function of the void fraction.

*Sometimes $1/C_m$ is referred to as the coefficient of virtual mass.

Equations 38 and 5 can be rewritten as

$$-1 = \rho_g a_{tp} \frac{du_g}{dP} + \frac{\rho_\ell a_{tp}}{C_m}\left(\frac{du_g}{dP} - \frac{du_\ell}{dP}\right) \tag{39}$$

and

$$-1 = \alpha\rho_g a_{tp} \frac{du_g}{dP} + (1-\alpha)\rho_\ell a_{tp} \frac{du_\ell}{dP} \quad , \tag{40}$$

respectively. It has been assumed here that the behavior of a given gaseous volume is characteristic of all gaseous volumes in the flow field, i.e., that du_g/dP in Eq. 39 is equal to du_g/dP in Eq. 40. As was discussed above, the rate of interphase momentum transfer is reflected by the term dk/dP. By definition

$$k = u_g/u_\ell \ . \tag{41}$$

such that

$$\frac{dk}{dP} = \frac{1}{u_\ell}\left[\frac{du_g}{dP} - k\frac{du_\ell}{dP}\right] \approx \frac{1}{a_{tp}}\left[\frac{du_g}{dP} - \frac{du_\ell}{dP}\right] . \tag{42}$$

Eqs. 39, 40, and 42 can be solved simultaneously to give

$$\frac{dk}{dP} = \frac{-1}{a^2_{tp}\rho_\ell}\left[\frac{(1-\alpha)(\rho_\ell - \rho_g)C_m}{(1-\alpha)\rho_\ell + \alpha\rho_g + (1-\alpha)\rho_g C_m}\right] . \tag{43}$$

This expression is representative of a discrete gaseous phase. Since there is no well-defined transition from liquid-continuous to gas-continuous systems, a void fraction of 0.50 will be set as an arbitrary maximum for the validity of Eq. 43. If the system conditions are restricted to moderate and low pressures such that $\rho_g << \rho_\ell$ and C_m is

assumed to be small (of order 1) compared to the density ratio (of order 100), then Eq. 43 can be simplified to

$$\frac{dk}{dP} = -C_m/a_{tp}^2\rho_\ell \tag{44}$$

Substitution of Eq. 44 into Eq. 37 gives

$$a_{tp} = \left[\frac{1 + \alpha(1 - \alpha)C_m}{\left[\alpha^2 + \alpha(1 - \alpha)\frac{\rho_\ell}{\rho_g}\right] + \left[(1 - \alpha)^2 + \alpha(1 - \alpha)\frac{\rho_g}{\rho_\ell}\right]\frac{nP}{\rho_g a_\ell^2}}\right]\frac{nP}{\rho_g} \tag{45}$$

or

$$\frac{a_{tp}^2}{a_{ht}^2} = [1 + \alpha(1 - \alpha)C_m]n. \tag{46}$$

The polytropic exponent n is a function of the rate of interphase heat transfer. As was shown in the discussion of the homogeneous models, one of two assumptions is employed to approximate the heat transfer, i.e., either complete ($n \tilde{\gtrless} 1$) or negligible ($n = \gamma$) heat transfer exists. The merits of each of these assumptions have been thoroughly discussed[2,7,9] and it has been generally agreed that, for void fractions where large bubble coalesence occurs, the gaseous volumes are so large that the thermal response is negligible compared to pressure response. Therefore, these large volumes essentially follow an adiabatic path. The existence of interphase heat transfer at very low void fractions ($\alpha < 0.10$), which implies small isolated bubbles, has been demonstrated.[9] In this instance, the polytropic path lies between the adiabatic and isothermal processes, and it appears to be a function of the void fraction. Thus, it is assumed that the exponent is a function of the void fraction and the isentropic exponent:

$$n = n(\alpha,\gamma). \tag{47}$$

Most of the investigations reported in the literature employed either air-water or steam-water mixtures as the working media. The gaseous phases of steam and air have roughly the same isentropic exponents; hence, the dependency of n:

$$n(\alpha)_{\gamma} \text{ is such that } 1 \leq n \leq \gamma; \tag{48}$$

$$n(\gamma)_{\alpha} \text{ is such that } 1.32 \leq n \leq 1.4, \tag{49}$$

with the void fraction is much greater than with the isentropic exponent. For such systems it is reasonable to assume

$$n = n(\alpha). \tag{50}$$

This means Eq. 35 can be expressed as

$$a_{tp}/a_{ht} = f(\alpha), \tag{51}$$

which implies that all the low-quality steam-water and air-water data may be correlated as a function of only the void fraction. This correlation combines the effects of interphase heat and momentum transfer.

D. Droplet Flows

The treatment of droplet flows is similar to that of bubbly flows. If it is assumed that the droplet is spherical, the momentum equation is

$$-\frac{dP}{dz} = \rho_{\ell} u_{\ell} \frac{du_{\ell}}{dz} - \frac{\rho_g}{2}\left(u_g \frac{du_g}{dz} - u_{\ell} \frac{du_{\ell}}{dz}\right). \tag{52}$$

If in addition it is assumed that the behavior of one droplet is characteristic of all droplets in the flow field, Eq. 52 can be combined with Eqs. 5 and 42 to give

$$\frac{dk}{dP} = -\frac{1}{\rho_g a_{tp}^2}\left[\frac{2\alpha}{(1+\alpha)+\alpha\frac{\rho_g}{\rho_\ell}}\right] , \tag{53}$$

which for low pressures ($\rho_g << \rho_\ell$) can be approximated by

$$\frac{dk}{dP} = -\frac{2\alpha}{a_{tp}^2 \rho_g (1+\alpha)} . \tag{54}$$

Since the liquid is essentially incompressible, any temperature change due to the passage of a wave front is negligible. Therefore, any interphase heat transfer is dependent upon the gas behavior. The large thermal capacity of the liquid ($\rho_\ell C_\ell$) determines that the heat-transfer process is governed by the transient conduction through the gas to the essentially constant-temperature liquid. For the large gas volumes commensurate with droplet flows, the thermal response of the gas can be neglected such that

$$\frac{d\rho_g}{dP} = \frac{\rho_g}{\gamma P} . \tag{55}$$

Substituting Eqs. 54 and 55 into Eq. 37 and neglecting the liquid compressibility gives

$$\frac{a_{tp}}{a_g} = \left\{\frac{1+\frac{2\alpha^2(1-\alpha)\rho_\ell}{(1+\alpha)\rho_g}}{\alpha^2+\alpha(1-\alpha)\frac{\rho_\ell}{\rho_g}}\right\}^{1/2} . \tag{56}$$

For $\alpha > 0.50$ this expression is closely approximated by

$$\frac{a_{tp}}{a_g} = \sqrt{\frac{2\alpha}{1+\alpha}} . \tag{57}$$

E. Separated Flows

This designation is used to represent any flow pattern in which the liquid and gaseous phases are both axially continuous, such as the stratified, annular, and filament flows illustrated in Fig. 4. These configurations will be treated for smooth and wavy interface conditions.

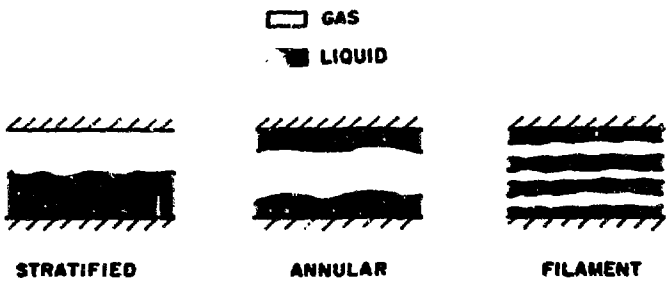

Fig. 4. Illustration of Simple Separated-flow Regimes

Although the formulations are one-dimensional, in a system such as an air-water mixture the mismatch between the acoustical impedances of the phases is considerable, and one must be aware of the two-dimensional aspects of the propagation. Davies[21] states that, in annular flow, each phase will transmit a pressure disturbance at its own propagation velocity. Such behavior is shown in Fig. 5a, and it is immediately apparent that this situation produces transverse pressure discontinuities which cannot exist. The relaxation of these discontinuities produces a transverse motion similar to that experienced by pressure waves propagating through a liquid contained in a flexible pipe.[24] It is proposed that these transverse forces skew the initially planar pulse into a configuration like that shown in Fig. 5b. When the depth of the liquid layer is much smaller than the length over which the pulse travels, the wave can be considered of constant shape and to travel

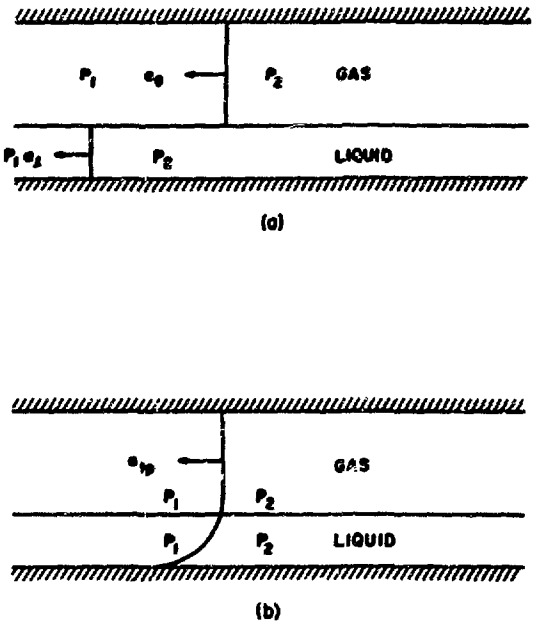

Fig. 5. Illustration of (a) Possible Nonuniform Propagation and (b) Resulting Wave Form for a Simple Stratified Media

with a single velocity. It is this velocity that the following derivations are concerned with, and all the approximations made must be considered in light of this two-dimensional flow pattern.

1. Smooth Interface

For smooth-interface conditions, such as the configuration shown in Fig. 5b, there is no virtual mass associated with either of the phases and the viscous momentum transfer can be neglected in the region near the wave front. Therefore, the momentum equations for the individual phases can be simply written as

$$\frac{dP}{dz} + \rho_g a_{tp} \frac{du_g}{dz} = 0 \tag{58}$$

and

$$\frac{dP}{dz} + \rho_\ell a_{tp} \frac{du_\ell}{dz} = 0 \ , \tag{59}$$

which can be rearranged as

$$\frac{du_g}{dP} = - \frac{1}{\rho_g a_{tp}} \tag{60}$$

and

$$\frac{du_\ell}{dP} = - \frac{1}{\rho_\ell a_{tp}} \ . \tag{61}$$

Equations 60 and 61 can be substituted into Eq. 42 to give

$$\frac{dk}{dP} = \frac{-1}{a_{tp}^2} \left(\frac{1}{\rho_g} - \frac{1}{\rho_\ell} \right) \ . \tag{62}$$

The separated-flow regimes have a considerably smaller interfacial area than the bubbly patterns; thus, one would expect much less heat transfer for these regimes. Since the large bubbles appear to exhibit an adiabatic behavior, it is reasonable to assume these separated patterns also experience a negligible rate of heat transfer.

The separated-flow patterns occur at qualities where the compressibility of the liquid is a negligible portion of the system compressibility; hence, the liquid may be considered incompressible, which is equivalent to an infinite propagation velocity for the liquid phase.

The three above conditions may be substituted into Eq. 37 to yield

$$a_{tp}^2 = \left\{ \left[\alpha^2 + \alpha(1-\alpha)\frac{\rho_\ell}{\rho_g} \right] \frac{\rho_g}{\gamma P} + \frac{\alpha(1-\alpha)(\rho_\ell - \rho_g)^2}{a_{tp}^2 \rho_g \rho_\ell} \right\}^{-1} ; \qquad (63)$$

this relationship may be rearranged to give

$$\frac{a_{tp}^2}{a_g^2} = 1 + \frac{(1+\alpha)^2 + \alpha(1-\alpha)(\rho_g/\rho_\ell)}{\alpha^2 + \alpha(1-\alpha)(\rho_\ell/\rho_g)} , \qquad (64)$$

which is easily reduced to

$$\frac{a_{tp}^2}{a_g^2} = 1 + \frac{1-\alpha}{\alpha}\frac{\rho_g}{\rho_\ell} . \qquad (65)$$

Eq. 65 is the one-dimensional expression for the propagation of a pressure pulse through a smooth-interface separated-flow regime where the effects of interphase heat, mass, and momentum transfer are negligible.

2. Wavy Interface

Separated-flow patterns, of which annular is the most common, are characterized by wavy interfaces.[25] These surface waves also experience a virtual mass effect when there is relative acceleration with respect to the gaseous core. The effect of surface waves will be investigated by analyzing a case in which the wave amplitude is large compared to the minimum film thickness, such as the configuration shown in Fig. 6. It is assumed that such a geometry can be approximated by hemicylindrical filaments resting on the surface. For a cylindrical rod in cross flow, the coefficient of virtual mass is equal to unity.[26] Therefore, the momentum equation for a given filament can be written as

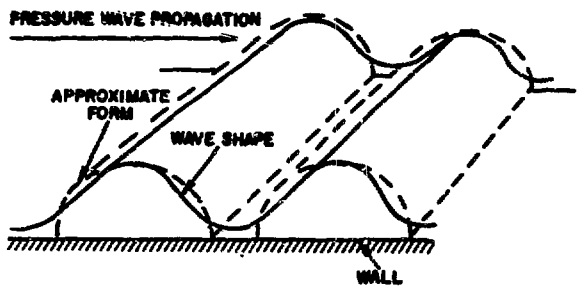

Fig. 6. Approximate Wave Form Employed to Describe Momentum Transfer in Wavy Annular Flow

$$-\frac{dP}{dz} = \rho_\ell u_\ell \frac{du_\ell}{dz} - \rho_g \left(u_g \frac{du_g}{dz} - u_\ell \frac{du_\ell}{dz} \right). \tag{66}$$

Following the procedure used for bubbly and droplet flows, one can derive the following expression for the propagation velocity in the approximate flow configuration shown in Fig. 6:

$$a_{tp}/a_g = \sqrt{\alpha}. \tag{67}$$

This formulation will be referred to as the wavy-interface model.

F. Mass-transfer Considerations for One-component Droplet and Separated-flow Patterns

The various momentum considerations discussed above are valid for both one- and two-component mixtures. However, the expressions given by Eqs. 57, 65, and 67 are based on negligible rates of interphase mass transfer. As discussed in the section on bubbly flows, this is a good approximation for such low-quality one-component flows, but it may not be equally applicable to other flow patterns.

Considerable effort has been directed toward analyzing pressure wave propagation in reacting gas mixtures,[27,28] which is a problem closely allied with those considered herein. The major conclusion of these studies is that for any finite reaction rate, the wave front propagates in a frozen (no mass transfer, $dx/dP = 0$) manner. This particular conclusion is substantiated by some very ingenious and detailed shock-wave data taken in a supersonic nozzle.[29] Other important conclusions of Refs. 27 and 28 are that the amplitude of the wave front decays rapidly and the bulk of the wave travels at some velocity less than the frozen speed. It is shown in Ref. 28 that for times

$$t >> \frac{2\lambda}{\frac{a_f^2}{a_e^2} - 1} \tag{68}$$

the bulk of the wave travels at a velocity close to that given by an equilibrium mass-transfer formulation. Therefore, an experimental investigation which claims to have measured frontal velocities may actually be measuring bulk wave velocities.

When the frontal velocity is considered in the light of the decaying amplitude and the two-dimensional aspects discussed above and illustrated in Fig. 5, it seems reasonable that the bulk velocity is the practical quantity to deal with when describing the overall one-dimensional behavior of a liquid-vapor system. Thus, the following solutions are intended to represent the bulk wave behavior in a given flow configuration.

As shown by Eq. 68, to determine the effects of mass transfer one must have a knowledge of the reaction (mass transfer) rate. To obtain such information for a two-phase system requires an understanding of the governing processes and the interfacial surface area. The latter requirement demands a detailed picture of the flow configuration, which is the general unknown in two-phase flow. Therefore, one cannot present quantitative models, but by considering the nature of the processes and the general flow pattern, approximate solutions can be generated which give added insight into the overall one-dimensional behavior of one-component, two-phase systems.

The nature of interphase mass transfer differs considerably between compression and rarefaction waves. A compression wave propagating through a mixture initially in equilibrium produces superheated vapor and subcooled liquid, which are each individually stable states. To relax to equilibrium, the liquid must first be heated by the vapor, which is a process essentially controlled by conduction in the vapor. Thus, the case of one-component compression waves is very similar to that for two-component flow. In contrast, rarefaction waves generate superheated liquid and supersaturated vapor, which are both metastable states and each may relax independently of the other. Such a relaxation for the vapor requires condensation which, in turn, requires a nucleation site. The liquid temperature is greater than that of the vapor; hence, the liquid phase cannot serve as the site. As illustrated by the condensation shocks witnessed in the flow of saturated vapor through converging-diverging nozzles, vapor can be considerably supersaturated before any spontaneous relaxation to equilibrium is initiated.[30] Therefore, it will be assumed that in the wave front no condensation exists and the vapor behaves isentropically as if it were superheated steam ($\gamma \approx 1.3$). The superheated liquid vaporizes as it relaxes to a stable equilibrium condition. Since there is a definite waiting time involved in the growth of vapor bubbles, it is assumed no bubbles are formed within the liquid phase. Thus, the vaporization occurs at the interface. Vaporization at the liquid interface yields a surface temperature equal to the local saturation value, which remains essentially constant regardless of the amount vaporized. The response of the liquid phase

and the mass transfer are thus governed by the conduction response of the liquid volume with the imposed boundary condition of constant temperature.

As outlined above, the interphase mass-transfer rate is governed by the transient conduction response of the vapor and the liquid to compression and rarefaction waves, respectively. For identical geometries, the transient conduction response of water is faster than that of steam by more than two orders of magnitude. For typical annular and mist flows, the vapor volume fraction is greater than that of the liquid by one order of magnitude. Hence, the transient response of the liquid is 1000 times faster than that of the vapor. On the basis of these estimates, it is assumed that the transient conduction response of the vapor is negligible ($dx/dP = 0$), and the solutions for compression waves propagating through one-component annular, wavy-annular, and mist flows are identical to the two-component solutions presented above. (One possible exception will be discussed in Ch. 5.) However, the mass-transfer response in rarefaction waves requires further consideration.

As was discussed above, the rate at which the mass transfer occurs is dependent on the nature of the process and the area available for transfer. For rarefaction waves the mass transfer has been equated to the rate at which liquid conducts heat to the interface:

$$q = - K_\ell A_s \left.\frac{dT_\ell}{dy}\right)_{surface} \tag{69}$$

where A_s is the interfacial surface area for a given mass of liquid and $\left.dT_\ell/dy\right)_{surface}$ is the temperature gradient at the surface. For heat-transfer purposes two geometries are considered herein: thick films (smooth and wavy separated flows) and small droplets (mist flows). The surface area for mist flows can be one to three orders of magnitude greater than that for the separated configurations. Hence, if the interphase mass transfer is appreciable, the effect will be most noticeable in the mist-flow regime. Therefore, it is assumed that the

mass-transfer rate for films is negligible because of their comparatively small surface area and thick geometry, but that the rate for small droplets can be approximated by the equilibrium rate for vaporizing liquid. Therefore, the rarefaction-wave models for smooth and wavy separated flows are identical to the two-component solutions. For mist flows, the total system and vapor entropies are assumed constant such that

$$ds_o = d[(1 - x)s_f + xs_g] = 0 \ , \tag{70}$$

and the mass-transfer rate can be expressed by

$$\frac{dx}{dP} = - \frac{(1 - x)}{S_{fg}} \frac{ds_f}{dP} \ . \tag{71}$$

Hence, the mist-flow solution for rarefaction waves can be expressed as

$$a_{tp} = \left\{ \frac{\dfrac{1 + 2\alpha^2(1 - \alpha)\rho_f}{(1 + \alpha)\rho g}}{[\alpha^2 + \alpha(1 - \alpha)(\rho_f/\rho_g)]/a_g^2 + \rho_f \dfrac{\alpha(1 - \alpha)}{xs_{fg}} \dfrac{ds_f}{dP}} \right\}^{1/2} \ . \tag{72}$$

In summary, considerations of the interphase mass-transfer characteristics has led to the following approximations for the rate of mass transfer in compression and rarefaction waves:

(1) For compression waves, the interphase mass transfer is governed by the conduction response of the vapor, which is a comparatively slow process. Thus, it was assumed the mass-transfer rate was negligible and the solutions for the three flow patterns considered are the same as for the two-component models.

(2) For rarefaction waves, the liquid conduction response controls the mass transfer. This is a much faster process; however, it was assumed the small surface area and thick geometry of the separated flows

severely restricted this response and the mass-transfer rate was negligible. Hence, these two models are also the same as their two-component counterparts. For mist flows, the large interfacial area and minute geometries were considered conducive to large mass-transfer rates. An equilibrium liquid-vaporization solution was assumed for these flows.

G. Slug Flow

The two-phase slug-flow pattern normally consists of elements of liquid which completely fill the cross section of the flow channel and regions of vapor which, except for a thin liquid film on the wall, also occupy the flow channel as shown in Fig. 7a. A region of bubbles which normally trails the vapor region in a flowing slug system is not shown and is neglected in the discussion that follows. The slug-flow regime presents a somewhat different situation than those flow regimes previously discussed. This difference arises from the fact that neither the vapor nor liquid region can be considered continuous over an extended length of flow channel. This assumes, in line with Fig. 5b, that the liquid film on the wall in the vapor region does not provide continuity for pressure-pulse propagation in the liquid phase. As previously discussed, a smooth stratified or annular region has a propagation velocity equal to that of the vapor phase alone. Therefore, an approximate slug-flow element is considered in which the vapor region completely fills the channel, as shown in Fig. 7b.

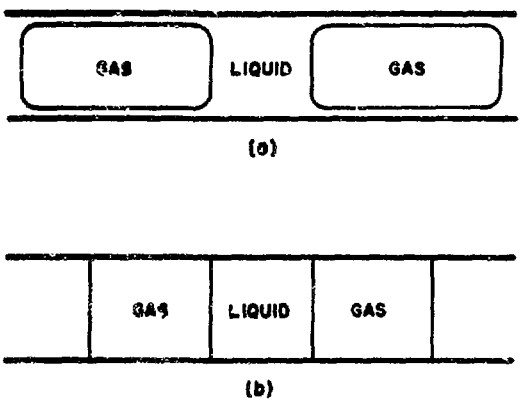

Fig. 7. Gas and Liquid Elements in (a) a Slug-flow Pattern and (b) Idealized Slug-flow Model.

The discontinuous nature of the slug-flow regime requires a somewhat different approach in discussing the response of this system to pressure pulses. Three important concepts are discussed in this section:

i pressure-pulse propagation in each phase;

ii attenuation of pressure pulse on crossing a vapor-liquid interface (i.e., transmitted and reflected pulses);

iii total response of the vapor element to a step change in pressure.

Consider the simplified illustration of the slug-flow pattern in Fig. 7b; elements of slug flow of length L consist of regions of liquid of length L_ℓ and of vapor of length L_v. The total time t for the front of a pressure pulse to transverse one element of vapor and liquid is related to the propagation velocity in each phase:

$$t = \frac{L_\ell}{a_\ell} + \frac{L_g}{a_g} \quad . \tag{73}$$

If in a given length of slug flow the total length is written as the sum of the elements of gas and liquid,

$$L = \Sigma L_\ell + \Sigma L_g \quad ; \tag{74}$$

the liquid and vapor volume fractions respectively are taken as

$$\alpha = \frac{\Sigma L_g}{L} \; ; \quad 1 - \alpha = \frac{\Sigma L_\ell}{L} \quad . \tag{75}$$

It then follows that the propagation velocity of the front of a pressure pulse can be written as

$$a_{tp} = \left(\frac{\alpha}{a_g} + \frac{1 - \alpha}{a_\ell} \right)^{-1} \quad . \tag{76}$$

To give further understanding of slug flow it is necessary to consider the transmission of a pressure pulse across a vapor-liquid

interface. As discussed in Ref. 31 the conditions at the boundary of two media, i.e., vapor and liquid, are

i The total pressure must be equal at the interface.

ii The particle velocity into the interface must equal the particle velocity out of the interface.

The first condition is a requirement that pressure be continuous across the boundary. The second implies a condition that the two media remain in contact. This leads to the condition that the ratio of the amplitude of the transmitted pressure pulse to the amplitude of the incident pressure pulse is given by

$$\frac{\Delta P_\ell}{\Delta P_g} = \frac{2}{1 + \frac{\rho_g a_g}{\rho_\ell a_\ell}} \tag{77}$$

for a pulse transmitted into the liquid from the vapor, and by

$$\frac{\Delta P_g}{\Delta P_\ell} = \frac{2}{1 + \frac{\rho_\ell a_\ell}{\rho_g a_g}} \tag{78}$$

for a pulse transmitted into the vapor from the liquid. Thus a pressure pulse can be transmitted from the vapor to the liquid element with little attenuation, but is severely attenuated in transmission from the liquid to the vapor element. The net effect of importance in slug flow is that pressure-pulse propagation over several elements of slug flow is not a serious question at low pressures because of the severe attenuation on crossing the first liquid-vapor interface. Therefore, a different mode of pressure propagation may be considered in which the time required for the gas to respond to a step change in pressure in the liquid element is primarily determined by the inertia of the liquid. This pressure response

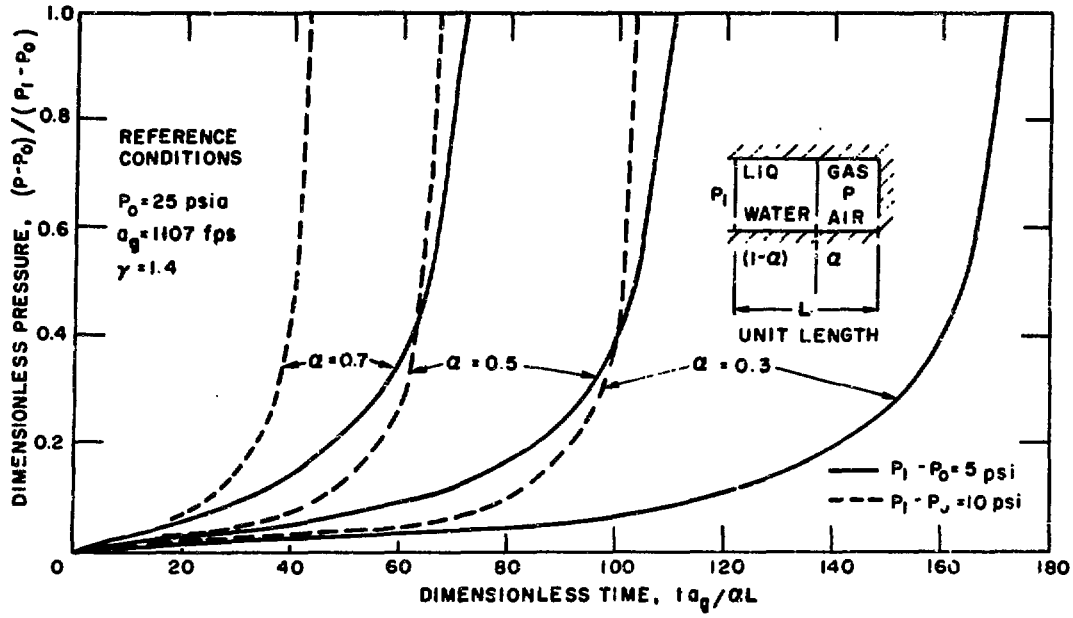

Fig. 8. Pressure Response of Gas Element in Slug Flow to Step Change Ahead of Liquid Element

is considered for an ideal liquid-vapor element shown in the insert to Fig. 8, where

L = length of element

L_g = length of vapor region

L_ℓ = length of liquid region

can be computed from the following equations:

$$\frac{P_\ell - P}{\rho_\ell L_\ell} = \frac{d^2 z}{dt^2} \tag{79}$$

and

$$\frac{dP}{\gamma P} = \frac{dz}{L_g - z} \tag{80}$$

with initial conditions

$$P_{t=o} = P_o \text{ and } Z_{t=o} = 0. \tag{81}$$

The pressure P is the pressure in the vapor region.

Eq. 79 describes the motion of the liquid element in the absence of friction, and Eq. 80 describes the adiabatic compression of the vapor element. In both equations, z is the location of the liquid-vapor interface. These equations were solved numerically, and typical results are shown in Fig. 8, where the normalized pressure response in the vapor $(P - P_o)/(P_\ell - P_o)$ is presented as a function of time. The time is made dimensionless with respect to the characteristic acoustic time $\alpha_o L/a_g$ for initial length of the vapor element. It is seen in Fig. 8 that the pressure response depends on the initial vapor volume fraction α_o and the magnitude of the step change in pressure. For the cases shown, it is seen that the time required for the pressure in the vapor to equal the step change in pressure is from 50 to 200 times larger than the characteristic acoustic time of the initial vapor volume. Except for very large pressure changes and/or small liquid volume fractions, the inertia of the liquid causes the total response to pressure to be much slower than any time for acoustic propagation in the vapor phase.

This discussion indicates that for the slug-flow case, two facts are important: 1) pressure waves traveling at the acoustic velocity of each phase are severely attenuated at the first crossing from liquid to gas, and 2) the response to a step change in pressure is determined by the inertia of the liquid element in the usual void-fraction range for slug flow and is much greater than the characteristic acoustic wave time L_g/a_g.

In this chapter, analytical developments have been presented for several distinct flow regimes. These models emphasize the effect of flow pattern on interphase momentum transfer and consequently on the system compressibility. The effect of flow regime and wave type on the inter-

phase mass transfer is considered for one component mixtures. The various models and their pertinent assumptions are summarized in Table I. Finally, the nature of pressure propagation in slug flows was studied for both acoustically and inertially limited cases.

TABLE I. Propagation Models for Liquid-Gas and Liquid-Vapor Mixtures

FLOW PATTERN[a]	HEAT TRANSFER	MASS TRANSFER	MOMENTUM TRANSFER	MODEL
BUBBLY 2C - C,R 1C - C,R	Correlated as a function of α	negligible	Correlated virtual mass of bubble as a function of α	$a_{tp} = f(\alpha) a_{ht}$
DROPLET 2C - C,R 1C - C	negligible	negligible	Virtual mass of droplet	$a_{tp} = a_g \sqrt{\frac{2\alpha}{1+\alpha}}$
DROPLET 1C - R	negligible	Equilibrium liquid evaporation	Virtual mass of droplet	Eq. 72
SEPARATED SMOOTH INTERFACE 2C - C,R 1C - C,R	negligible	negligible	negligible	$a_{tp} = a_g \sqrt{1 + \frac{1-\alpha}{\alpha} \frac{\rho_g}{\rho_\ell}}$
SEPARATED WAVY INTERFACE 2C - C,R 1C - C,R	negligible	negligible	Virtual mass of hemi-cylindrical waves	$a_{tp} = a_g \sqrt{\alpha}$
SIMPLE SLUG	-	-	-	$a_{tp} = \left(\frac{\alpha}{a_g} + \frac{1-\alpha}{a_\ell} \right)^{-1}$

[a] 1C - one-component mixture

2C - two-component mixture

C - compression wave

R - rarefaction wave

IV. EXPERIMENT

The experimental data of this study were obtained with the basic apparatus shown schematically in Fig. 9. The test loop was designed for the upward flow of both air-water and steam-water mixtures primarily in the low-void-fraction bubble-flow range. System pressures up to 65 psia in air-water and up to 50 psia in steam-water flows could be maintained.

The circulating pump and bypass arrangement provided water flow rate and control such that when combined with gas flow from the mixer, mixture velocities in the vertical test section were in the range from 1/2 to 1 fps.

The mixer section, shown in Fig. 10, was used for both air and steam injection. Mixing was obtained through use of a porous stainless steel filter with a factory-rated mean pore size of 20 μ. The gaseous phase was injected perpendicular to the water flow as recommended in Ref. 35. This arrangement provided steady "bubble" flow up to 40%

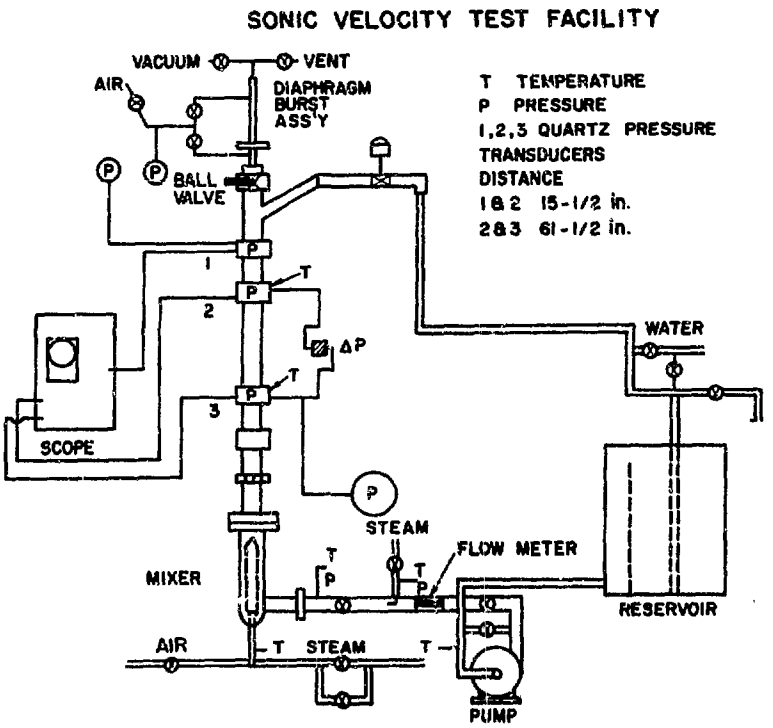

Fig. 9. Experimental Facility

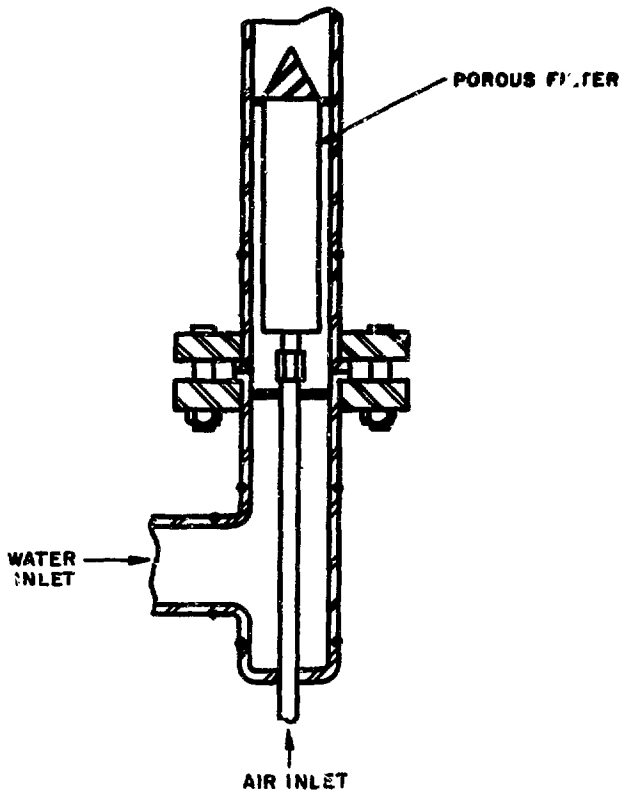

Fig. 10. Mixer Section for Experimental Facility

vapor volume fraction in air-water mixtures and up to 30% vapor volume fraction in the steam-water mixtures. This type of mixer arrangement was found superior to a parallel gas injection attempted early in the experimental program, which tended to produce slugging and unsteady flows at much lower vapor volume fractions than those noted above. Air and steam were available from laboratory supply lines. In the steam-water tests, steam was also injected into the water flow between the pump and the mixer section. This injection served to preheat the water only. After this injection, water just upstream from the mixer section was normally subcooled by 5 to 10°F. Saturation conditions in the vertical test section were achieved in some part from the steam injection through the mixer and in some part as a result of pressure drop into the mixer section.

The active vertical test section was made with 2-in. (2.07-in. ID) stainless steel pipe with provision for flush-mounted, quartz piezoelectric pressure-transducer mountings located 15.5 and 61.5 in. apart, as shown in Fig. 11. These mountings also had openings for pressure and temperature measurements. This test section was also insulated during steam-water operation to prevent heat loss.

Compression or rarefaction pressure pulses were produced by pressurizing or evacuating the chamber above the test section, causing the rupture of various thicknesses of nominal 1-mil (0.001-in.) aluminum

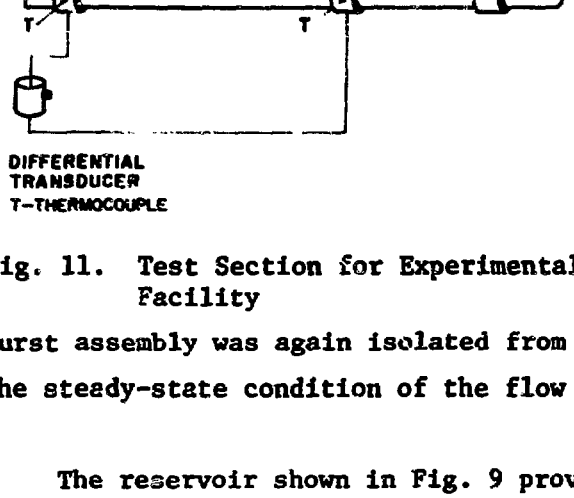

Fig. 11. Test Section for Experimental Facility

foil. Pressure pulses initiated in the diaphragm-burst assembly above the test section propagated downward into the two-phase mixture. Pressure pulses of 3- to 15-psi amplitude were produced in the air-water and steam-water flows. After the event, the upper diaphragm-burst assembly was again isolated from the main loop. Disturbance to the steady-state condition of the flow was only momentary.

The reservoir shown in Fig. 9 provided a constant reference pressure for what is essentially an open system. It is believed that this was helpful in maintaining overall loop stability, especially during steam-water operation. The reservoir also provided for gas separation in the air-water tests and deaeration of the supply water in the steam-water tests.

Temperatures were measured around the loop with sheathed iron-constantan and chromel-alumel thermocouples, calibrated in an oil bath up to 400°F against a platinum resistance thermometer (NBS standardized). Water, steam, and/or air pressures before the mixer section were measured with a single calibrated Statham transducer. The pressure drop between piezoelectric-transducer locations 3 and 2 was measured with a ±5-psid Statham differential transducer.

The void fraction was determined from the hydrostatic pressure between locations 2 and 3 (see Fig. 9). The hydrostatic pressure was calculated from the total pressure drop by correcting for the small effects of friction and momentum. In the steam-water studies correction was also made for the temperature difference between the test section and colder transducer leg. This provided a convenient measurement of the average void fraction in the test section between locations 2 and 3. Gamma-attenuation densitometry techniques were also used as a check in

the early stages of the experimental program. No discrepancies were found on comparing the measured void fraction by either method. However, the accuracy and sensitivity of the gamma-attenuation technique deteriorate at low void fraction much more rapidly than the pressure-drop method, so that the latter was used exclusively in reducing experimental data.

The quartz piezoelectric transducers used to record the pressure pulse at locations 1, 2, and 3 were Kistler model 603A type. These transducers were set in the mountings so as to be flush with the inside pipe wall when secured in place. The 603A transducers have a 0-3000 psi rise time of 1 μsec and a rated sensitivity of 0.05 psi. The output from the quartz transducers is converted to a voltage signal in the charge amplifier (Kistler model 503) and displayed on a Tektronix-Model 504 dual-beam memory oscilloscope. The arrangement is shown in Fig. 12. The output from transducer at location 1, closest to the diaphragm-burst assembly, was used to trigger the horizontal trace on the oscilloscope. The outputs from transducers at locations 2 and 3 were put into the vertical input amplifiers of the oscilloscope, which then displayed the pressure-time history at locations 2 and 3 from the instant that the pressure pulse passed location 1. A typical trace for the low-void-fraction steam-water flow is shown in Fig. 13 for a compression and superposed rarefaction pulse at approximately similar conditions. At time t_o the scope trace begins as the pulse passes location 1, both traces displaying the pressure at locations 2 and 3 respectively. At time t_1 the pressure pulse passes the transducer at location 2, as indicated by the sudden vertical deflection in the scope. After the passing of the front, the decay of the pulse is shown. The pulse does not reach location 3 until time t_2, where the sharp rise and gradual decay is similar to that at location 2. The propagation speed is taken as

$$a_{tp} = \frac{t_2 - t_1}{d_{2-3}} ,$$

where t_2 and t_1 are taken as the time characteristic of the front of the wave, and d_{2-3} is the distance between locations 2 and 3. Time

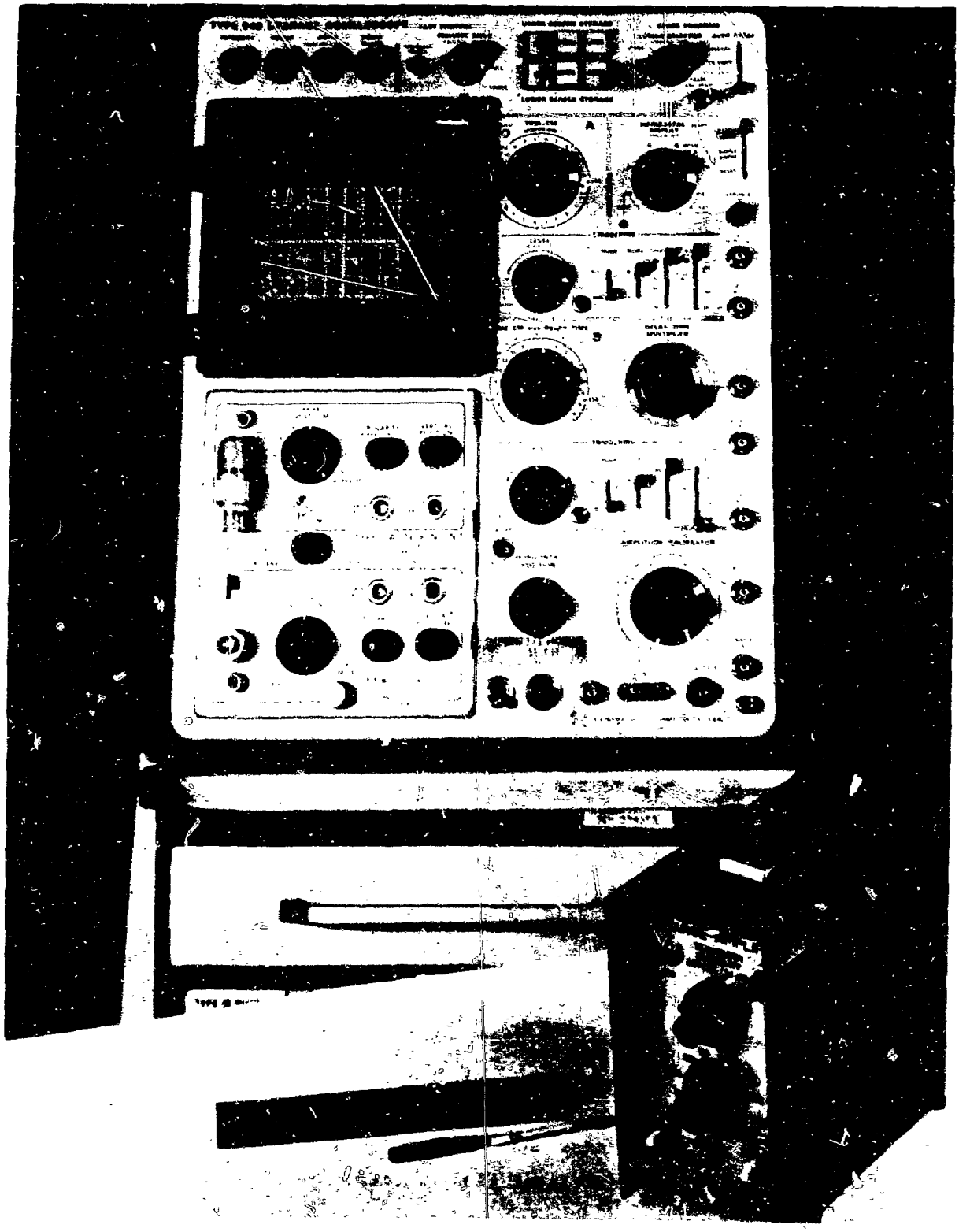

Fig. 12. Photo of Transducer, Oscilloscope, and Charge Amplifier. ANL Neg. No. 113-2786.

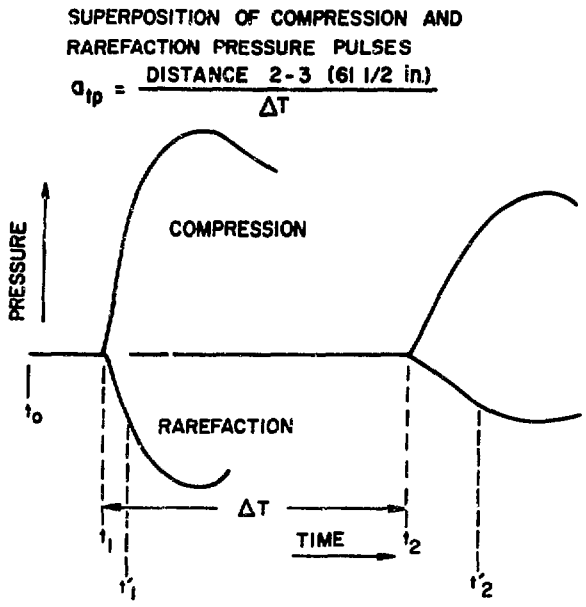

Fig. 13. Sample Oscilloscope Traces for Steam-water Compression and Rarefaction Pulses

characteristics of later stages of the pulse, such as $t'_2 - t'_1$, in these studies are somewhat slower and are discussed later in Chapter V.

The bubble-flow data were obtained in the flowing system Fig. 9. In the steam-water tests saturation conditions were achieved prior to the bursting of the diaphragm, for temperatures and pressures at locations 2 and 3 matched those of the Steam Table.[32]

The "slug" flow regime was approximated by a column of water standing in the test section at various levels between transducer locations 2 and 3. In this case, the void fraction, α, is a measure of the volume fraction of air between locations 2 and 3. The fractional height of liquid was varied from 0 to 1, and measurements of pressure-propagation velocity were obtained throughout the range with the pressure pulse initiated in the gas above the liquid.

The stratified regime was obtained by placing the test section in a horizontal position. For this study, the diaphragm assembly was mounted on the branch of the test section. The test section was rotated so that tests could be performed with the quartz transducers both in the bottom of the horizontal test section under liquid and on the top in the gas phase. Comparison of these two procedures is noted in the discussion of Ch. V.

The basic test apparatus thus allowed the comparison of experimental data in markedly different flow regimes. The results are discussed in Ch. V.

V. DISCUSSION OF THE RESULTS

The individual flow-regime analyses set forth in Ch. III were experimentally tested for bubbly, stratified, and slug-flow regimes using both steam-water and air-water mixtures. The experimental results will be separated and discussed on the basis of the flow patterns. The theories and experimental data of this investigation will then be compared to similar one- and two-component results which have appeared in the literature.

A. Bubbly Flow

The theoretical analysis of bubbly-like two-phase mixtures resulted in Eq. 51, which states that the ratio a_{tp}/a_{ht} can be correlated as a function of the void fraction. Figure 14 shows the air-water data taken at various system pressures. The correlation with void fraction is readily apparent. Any dependency on the system pressure is within the

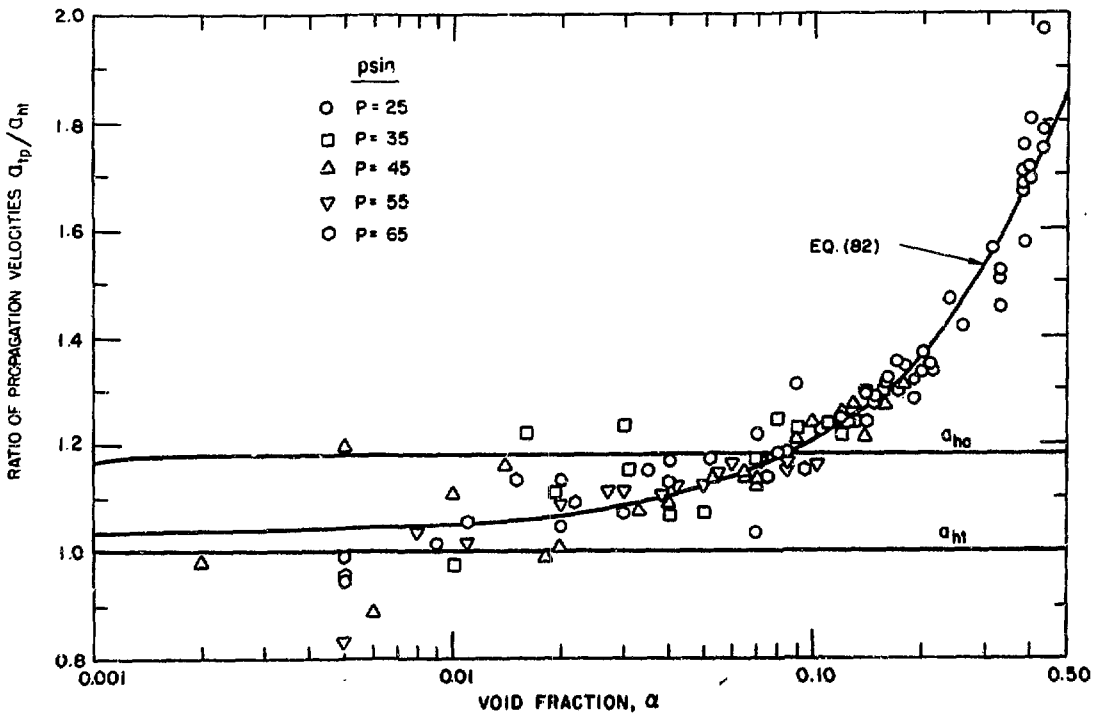

Fig. 14. Correlation of Air-water Data at Various Pressures

scatter of the data. The excellent correlation of the air-water results gives substantial justification to the virtual-mass mechanism and the validity of the assumptions employed in deriving Eq. 51. In order to facilitate the comparison of these air-water data to other results, the data were fit to a linear equation with a least-squares technique, giving

$$\frac{a_{tp}}{a_{ht}} = 1.032 + 1.676\alpha \tag{82}$$

The steam-water experimental results are compared to Eq. 82 in Fig. 15. The air-water correleation definitely lie within the scatter of the one-component data. The scatter in the steam-water system is larger than that of the two-component medium because it is more difficult to maintain a uniform mixture.

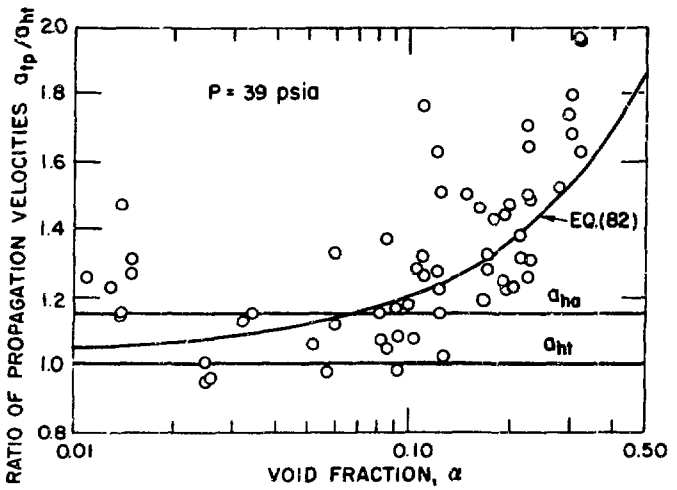

Fig. 15. Comparison of the Proposed Correlation and the Steam-water Data

Figure 16 illustrates the measured velocities of wave-front propagation and typical pressure-time traces for the compression and rarefaction waves employed in this study. As has been discussed in Ch. III, one would expect compression and rarefaction waves to exhibit different mass-transfer rates. This influence on the mass transfer is shown in Fig. 16. The portions of the wave traces which are well removed from the frontal zone show that the rarefaction pulses travel with considerably slower velocities than do the compression waves, which indicates a greater rate of mass transfer in the rarefaction pulse. Consequently, if the mass-transfer process exerts a significant influence on propagation velocity of a wave front, one would expect different frontal velocities for

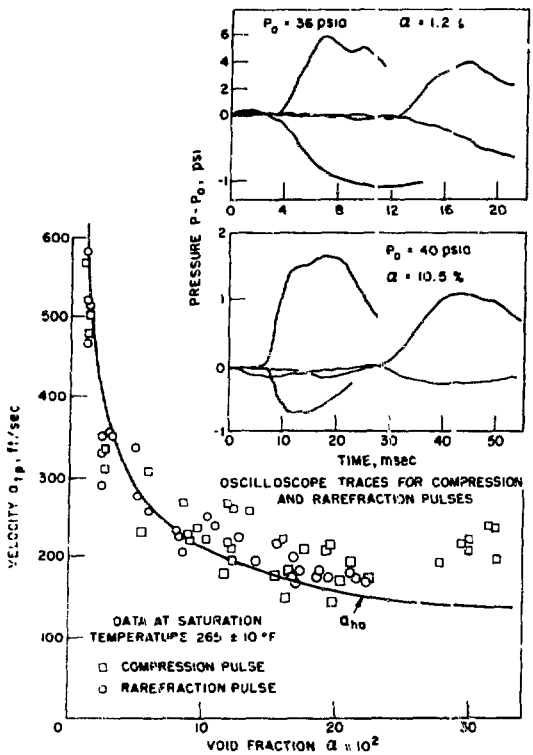

Fig. 16. Comparison of the Frontal Velocities for Compression and Rarefaction Waves in Steam-water Mixtures

compression and rarefaction pulses. As is shown in Fig. 16, any difference is within the experimental scatter of either type of pulse. Based on this evidence, it appears reasonable to assume that the wave front propagates with essentially no phase change ($dx/dP = 0$). This is in agreement with and provides additional verification for the negligible rate of mass transfer assumption employed in Ch. III.

The results of the experimental investigation substantiate the analytical development for bubbly flows which is presented in Ch. III.

The correlation given in Eq. 82, which is representative of the air-water data in this study, is compared to the results of other one- and two-component investigations in Figs. 17-20. The data shown are measurements of the velocities of wave-front propagation. As shown by Hamilton,[9] the propagation velocity is a function of the bubble size. Therefore, to compare Eq. 82 to the results of another system, one must assume that the mixing technique in that system generates approximately the same bubble patterns as those upon which the correlation is based. The general agreement exhibited in Figs. 17-20 shows that the formulation expressed by the derivation of Eq. 51 is a good average representation of the phenomenon of pressure-wave propagation in bubbly-like mixtures.

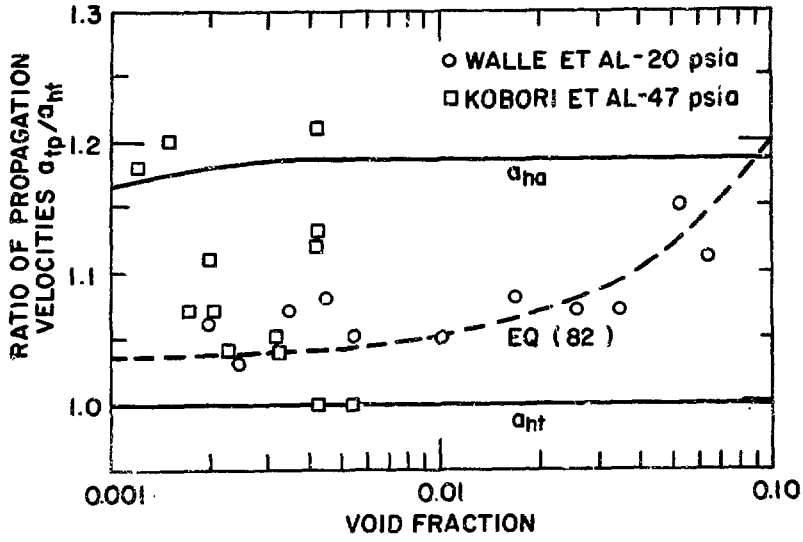

Fig. 17. Comparison of the Proposed Correlation and the Homogeneous Models with the Air-water Data of Refs. 13 and 33

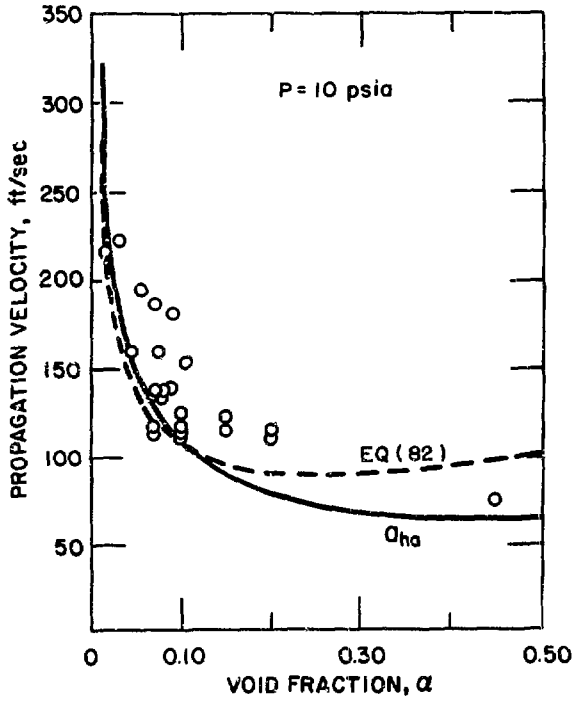

Fig. 18. Comparison of the Homogeneous Adiabatic Model and Eq. 82 with the Steam-water Data of Karplus

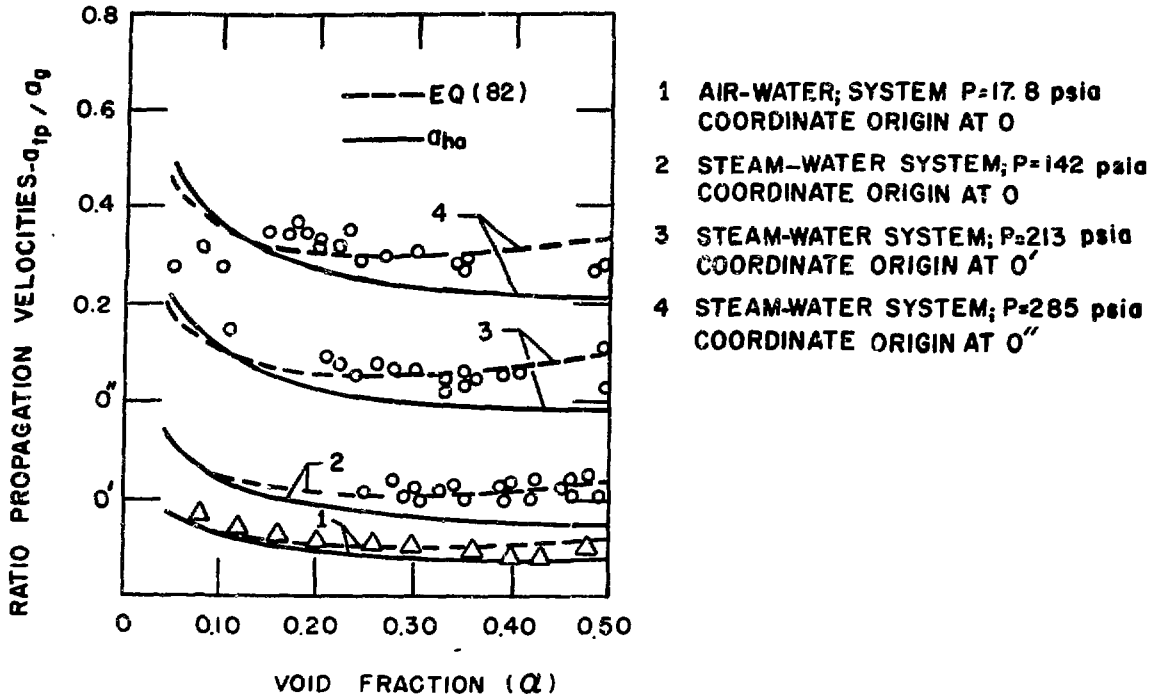

Fig. 19. Comparison of the Homogeneous Adiabatic Model and Eq. 82 with the Steam-water and Air-water Data of Semenov and Kosterin

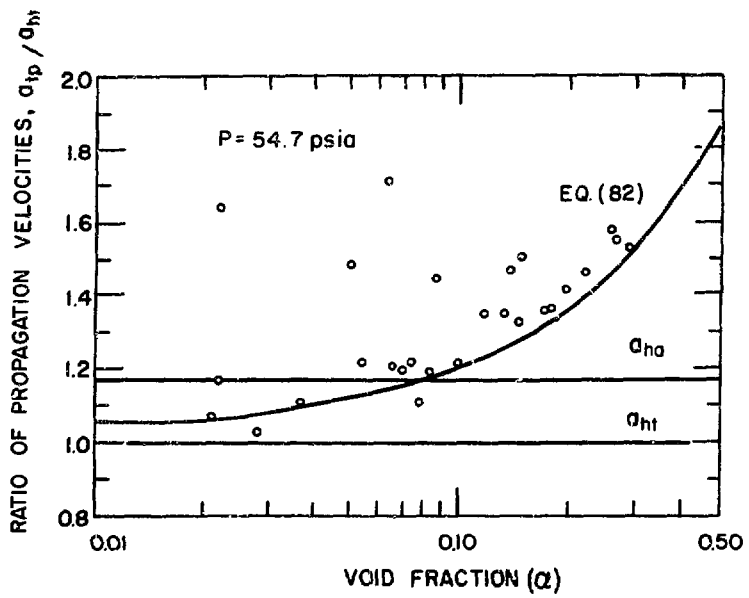

Fig. 20. Comparison of the Homogeneous Models and Eq. 82 with the Weak-shock-wave Air-water Data of Hamilton

The agreement between the air-water correlation of Eq. 82 and the high-pressure steam-water data shown in Fig. 19 contradicts the statement made in Ref. 12 that the Homogeneous Adiabatic Model predicts air-water behavior more closely than that of steam-water mixtures. According to the results in Fig. 19, the deviation from the Homogeneous Adiabatic Model is of the same relative magnitude, and the basis for the above statement was a consequence of the normalizing technique employed in representing the data at different pressures.

As was mentioned in Ch. II, the steam-water data reported by Hamilton[9] correspond to velocities which are considerably less than those of this and other such studies. Figure 21 shows a pressure-time trace taken from Ref. 9. The illustration compares the measurement technique used by Hamilton (intersection method) and that employed herein. It is seen that the different methods of interpretation yield quite different values of the time required for the wave to pass between the recording stations. In order to compare directly the results of the two studies, the three pressure-time traces given in Ref. 9 were evaluated by the method used in this study. Table 2 compares the results of the different evaluations with the correlation of Eq. 82 and shows that the data compare favorably if evaluated in the same manner. Therefore, the authors believe that the differences in the reported propagation velocities are generally due to the different data-reduction techniques employed.

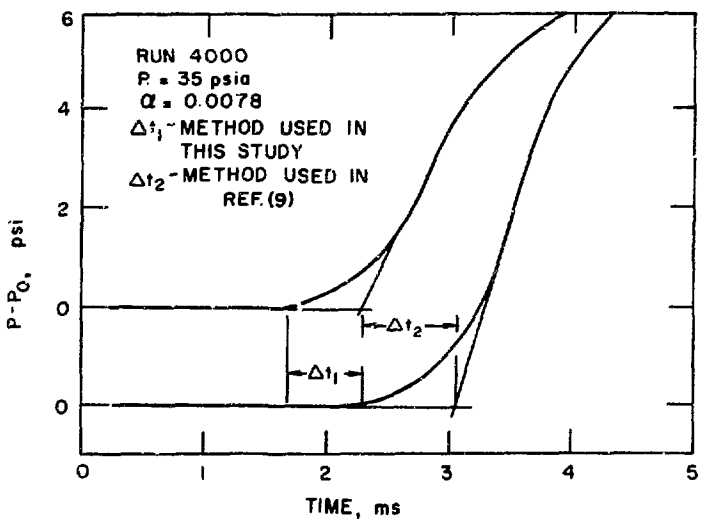

Fig. 21. Comparison of the Measurement Technique used in this Study and that Employed by Hamilton

TABLE II. Evaluation of One-component Data of Hamilton

Run	Void Fraction	Velocity Measured from Technique of Ref. 9 (ft/sec)	Velocity Measured from Technique of this Study (ft/sec)	Velocity Predicted from Eq. 82 (ft/sec)
4000	0.0078	398	666	625
3008	0.1760	113	123	182
4202	0.2140	151	208	203

Of the investigations discussed above, the results of Karplus[11] probably deviated the most from a uniform mixture because the bubbles were formed by boiling off a heater, and thus the bubbles were quite large. This set of data also exhibits the greatest scatter, which is the result of a lack of uniformity in the mixture. DeJong and Firey[14] also measured wave-front propagation velocities in liquid-continuous steam-water systems. Their results, which are shown in Fig. 22, exhibit higher velocities and more scatter than any of the other investigations discussed above. It is important to note here that the mixing technique employed was a parallel injection of steam into the mean water flow. This method produces considerably larger bubbles than the perpendicular injection technique discussed in Ch. IV and may have generated a flow regime which was not uniformly dispersed. The parallel injection was the original configuration used in this study, and the results were quite similar to those shown in Fig. 22. At the lower-void fractions, the mixture was well-behaved, there was little scatter in the data, and the results agreed well with those obtained using a perpendicular injection technique. For void fractions greater than 0.10, the scatter increased and the propagation velocities were consistently higher than those characteristic of the other mixing method. The increase in data scatter was accompanied by an increase in the oscillations of the static-head densitometer, which was indicative of an unsteady flow pattern and, thus, a lack of uniformity in the mixture.

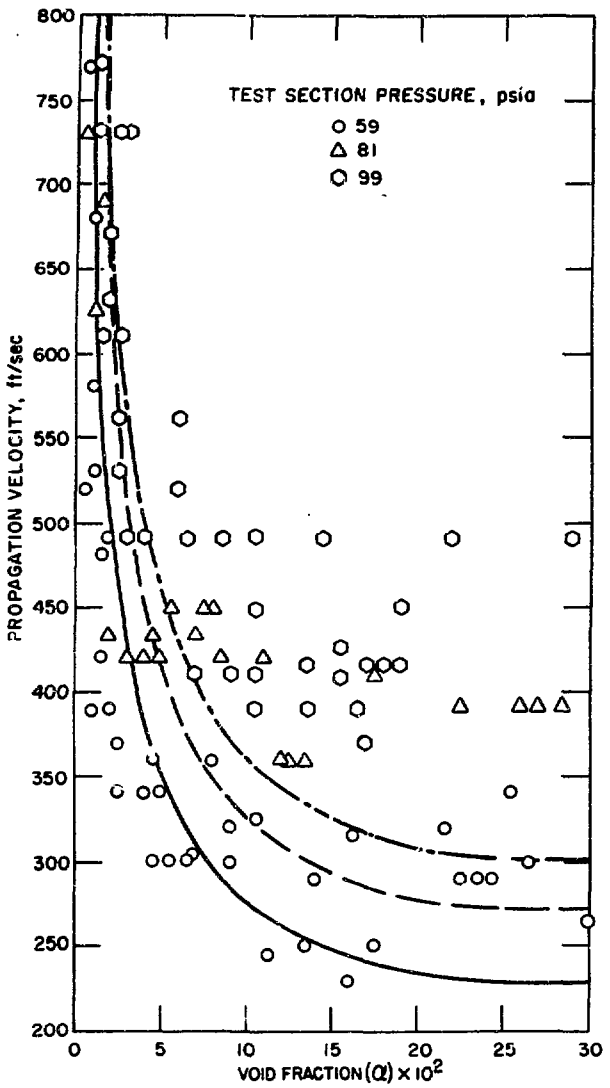

Fig. 22. Comparison of Eq. 82 and the Steam-water Data of DeJong and Firey

DeJong and Firey observed that the same pulse exhibited different propagation velocities in the upper and lower portions of the test section. This is, as mentioned in Ref. 14, also an indication that the flow pattern is not uniform, and, hence, is in agreement with the above discussion.

As has been discussed above, the rates of interphase heat, mass, and momentum transfer play a major role in the system compressibility. It was also seen that portions of a wave removed from the frontal zone may travel at velocities which are considerably different than the frontal speed, because the rate processes are different for the two regions. Therefore, it is reasonable to suspect that the velocity of sound for a two-phase mixture, which is the transmission of a continuous wave, will differ from the pressure-pulse propagation velocity characteristic of the same mixture. An infinitesimal pulse involves the thermal and mechanical response to a sudden change in pressure; the mechanical response is governed only by the inertial terms, and the thermal response is determined by the conduction solution to a rapid change in wall temperature.[34] However, the propagation of a sound wave involves the thermal and mechanical response to a continuously varying pressure, which implies that the mechanical

response is a function of both the inertial and viscous terms, and the thermal response time must be compared with the period of the wave. For a given amplitude, a lower frequency will allow more time to develop a relative velocity between the phases and, thus, a greater degree of momentum transfer because of the viscous terms, and it will also allow more time for interphase heat transfer. The result of increased heat and momentum transfer is a lower propagation velocity, which implies that two-phase sound propagation is a function of frequency with the lower frequencies having a slower propagation velocity; the limiting case of zero frequency should correspond to the homogeneous isothermal solution which assumes complete heat and momentum transfer. This is the behavior recorded by Karplus[35] and shown in Fig. 23. The propagation velocity of an infinitesimal pulse, as shown by Eq. 82, appears to be equivalent to that of a high-frequency wave. It is noteworthy that Eq. 82 predicts a minimum velocity for $\alpha \approx 0.30$ which, as shown in Fig. 24, is in agreement with the higher-frequency results of Karplus[35] if one linearly extrapolates the data for void fractions of 0.40 and 0.50.

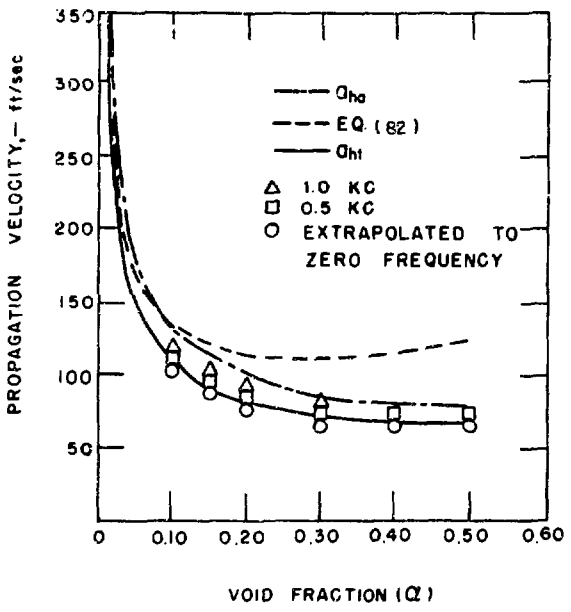

Fig. 23. Comparison of the Homogeneous Models and the Proposed Correlation with the Air-water Velocity of Sound Data of Karplus

In a one-component mixture, the propagation of a sound wave will exhibit a frequency dependence of even greater magnitude, because the rate of interphase mass transfer will also be frequency-dependent. Therefore, the distinction between the propagation velocities for an infinitesimal pulse and a sound wave will be even more dramatic.

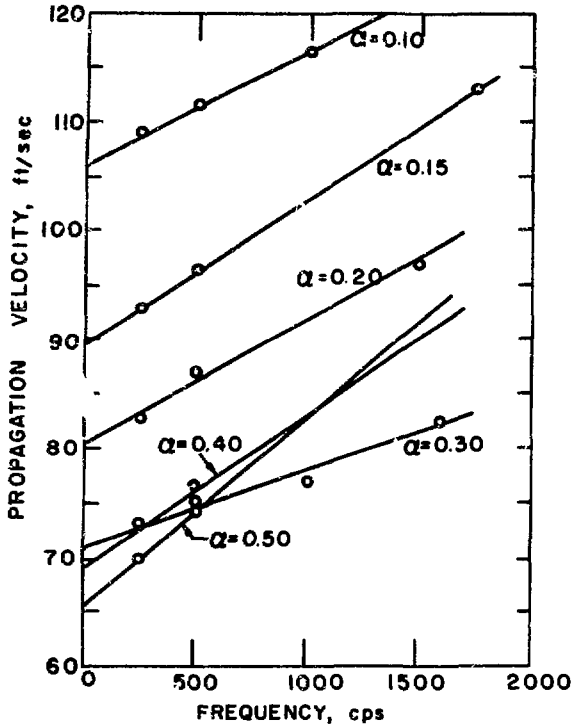

Fig. 24. Frequency Dependence of Velocity of Sound (Karplus[35])

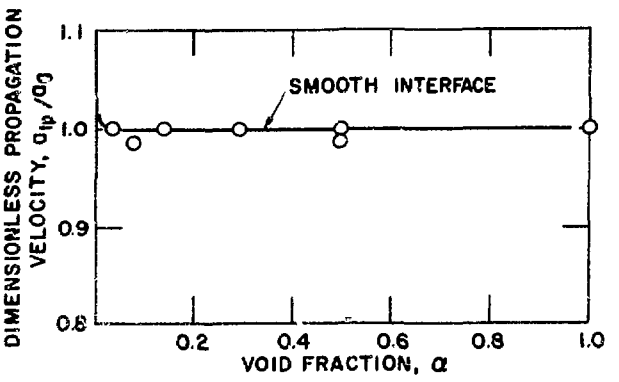

Fig. 25. Comparison of the Smooth-interface Model with the Stratified Air-water Data

B. Separated and Droplet Flows

Of the separated flow patterns illustrated in Fig. 4, only the smooth-interface stratified configuration was experimentally investigated in this study. The air-water data for compression and rarefaction waves are compared with the predictions of the smooth-interface model in Fig. 25. (All two-component data presented herein have been corrected for 100% relative humidity.) Excellent agreement is obtained. No difference was detected between compression and rarefaction waves, and no difference was found between measurements taken with the transducers in the liquid phase and those taken with the sensors in the gas. This latter point verifies the one-dimensional character outlined in Ch. III.

The steam-water stratified data is compared to the predictions of the smooth-interface, no-mass-transfer model in Fig. 26. It is readily apparent that the compression waves exhibit excellent agreement with the analytical prediction. The rarefaction waves also are in good agreement with the model; however, there is a small but consistent difference

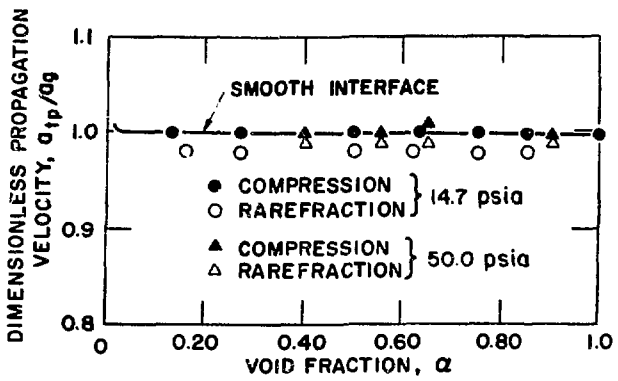

Fig. 26. Comparison of the Smooth-interface Model with the Stratified Steam-water Data. ANL Neg. No. 900-414 Rev. 1.

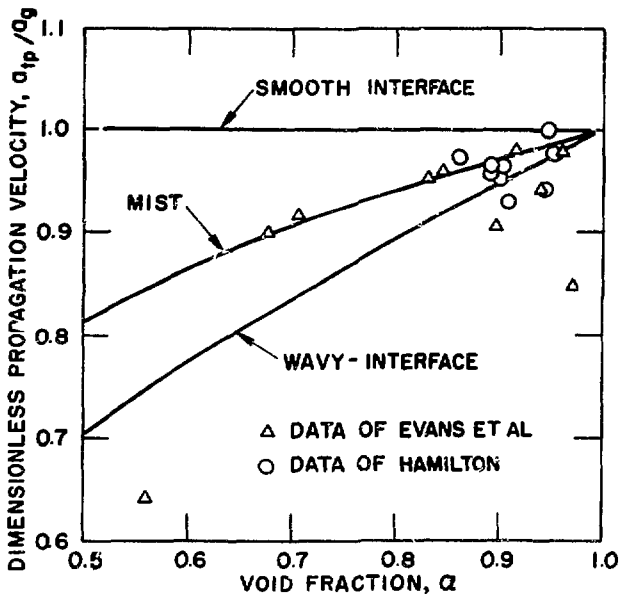

Fig. 27. Comparison of the Two-component Models with the Experimental Data of Refs. 7 and 9

between the two. This small discrepancy is probably the result of some surface evaporation, but since the conduction resistance of the liquid film is appreciable, the rate of mass transfer in the liquid is considerably less than the equilibrium value and, for all practical purposes, negligible as was assumed.

Evans et al.[7] and Hamilton[9] reported experimental two-component results for flows which are generally in the annular-dispersed or mist-flow regimes. These data are shown in Fig. 27 and are in general agreement with the predictions of the proposed models. Except at very low air velocities, films are relatively thin, which minimizes the wave amplitude. Therefore, one would expect better agreement with the droplet model than with the wavy-annular approach. The data and flow-regime observations of Ref. 7 substantiate such reasoning. The flow regime for the data point at $\alpha = 0.57$ should be approaching annular-slug transition and thus should contain large surface waves. Therefore, this particular point should be, and is, more closely approximated by the wavy-annular model.

The experimental air-water data of Garrard[17] are shown in Fig. 28a. The void fractions reported in Ref. 17 were determined from film-thickness measurements using wall-mounted conductance probes. Such measurements are insensitive to liquid entrained in the gaseous core. On the basis of the measurements reported by Hewitt,[36] it seems likely that the vertically upward flows described in Ref. 17 would experience some entrainment. To afford the reader a basis of comparison, the total liquid flow areas were estimated with the Lockhart-Martinelli[37] void-fraction correlation. The data are replotted as a function of the calculated total void fraction in Fig. 28b. For the thin wall films reported by Garrard, one would expect a relatively smooth annulus with entrainment in the core; thus, the data should be bracketed by the smooth annular and droplet models, which is indeed the case in Fig. 28b. Since the annulus contributes no momentum transfer, the droplet model and the data can be compared on the basis of the core void fraction. The void fraction in the dispersed core can be estimated by subtracting the liquid film area from the total liquid area predicted by the Lockhart-Martinelli correlation. This comparison is given in Fig. 28c; the experimental data are in good agreement with the droplet-flow prediction.

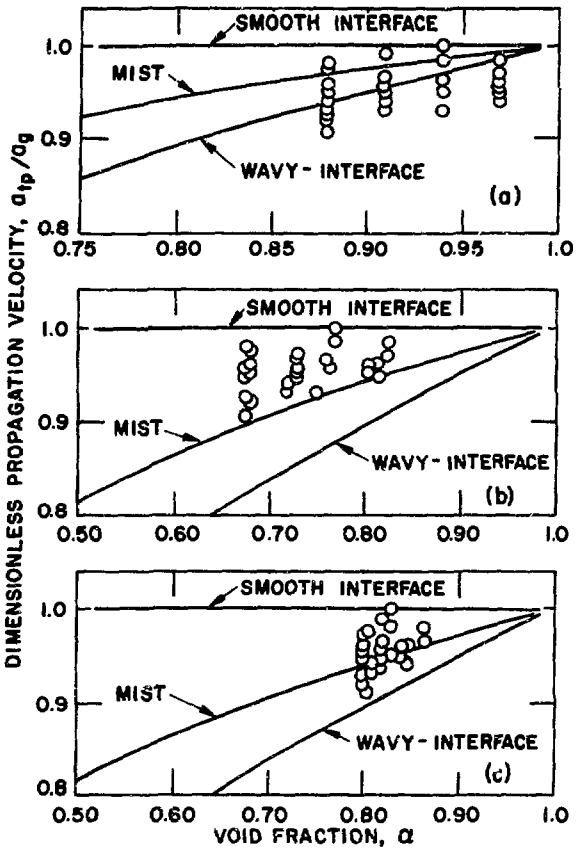

Fig. 28. Comparison of the Proposed Models with Air-water Data of Garrard for (a) Void Fractions Determined from Film Thickness Measurements, (b) Calculated Void Fractions, and (c) Calculated Core Void Fractions

White and D'Arcy[18] measured the propagation velocities of rarefaction waves in steam-water annular-flow systems. The mixer was designed to generate annular flows in a horizontal test section. No information is given about the shape of the interface in these flows; however, the smooth- and wavy-annular models should bracket the data. As is illustrated in Fig. 29, this is generally the case. (The void fractions were calculated by the authors using a correlation given in Ref. 38.)

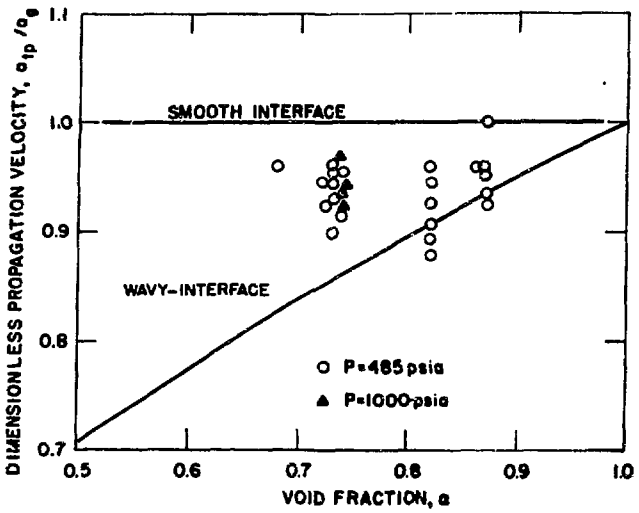

Fig. 29. Comparison of the Proposed One-component Models with the Steam-water Data of White and D'Arcy

Figure 30 compares the experimental results for compression and rarefaction waves propagating through a single phase medium (air) and a 50 percent quality steam-water mixture in a droplet flow pattern. These data, taken by DeJong and Firey,[14] clearly illustrate the difference in the propagation phenomenon between the two media. The one-component mist-flow models developed herein show excellent agreement with the measured velocities of small amplitude waves.

Figure 31 compares the predictions of models and the experimental data of England et al.[16] for rarefaction waves propagating through steam-water droplet flows. (Since the single-phase propagation velocity is slightly dependent on the air content in the steam, which was not specified, a_g was taken to be the average value measured in slightly superheated steam.) Again there is generally good agreement. As stated in Ref. 16, at the lower qualities ($x \sim 0.20$), some liquid was forming on the wall, thus decreasing the rate of interphase mass transfer. For such flow regimes, the data should be bracketed by the mist and annular predictions, which is indeed the case. In fact, since the wall film

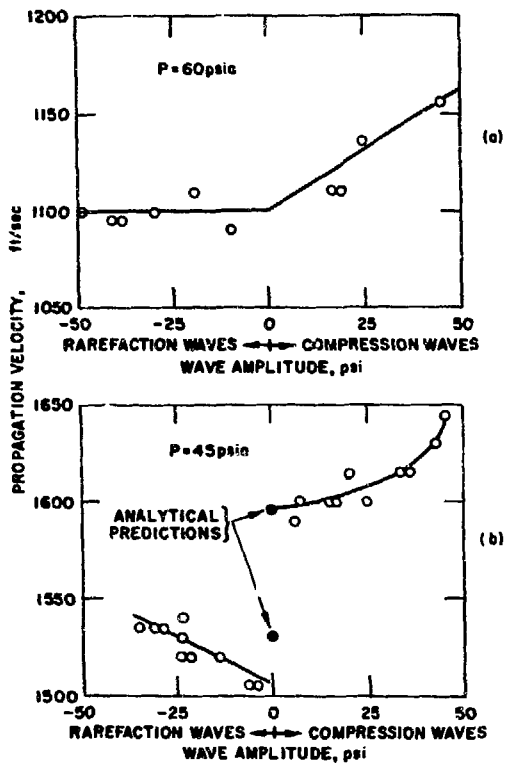

Fig. 30. Compression and Rarefaction Wave Data for (a) Air at 60°F and (b) a 50% Quality Steam-water Mixture as Reported in Ref. 14

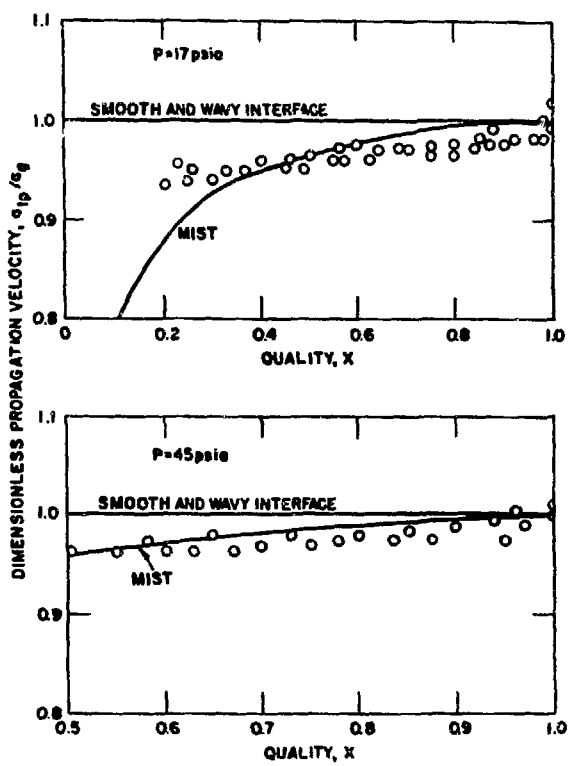

Fig. 31. Comparison of the One-component Models with the Rarefaction Wave Data of England et al.

contributes no mass transfer, one would expect that propagation velocities for annular-dispersed flows could be calculated based on the mixture quality in the dispersed core. This is substantiated in Fig. 32, which exhibits the experimental results of Collingham and Firey[15] for rarefaction waves propagating through annular-dispersed steam-water mixtures. The data are reported as functions of both gross and core qualities. As seen in Fig. 32, the data are bracketed by the mist and smooth-interface predictions as a function of gross quality, and the mist-flow model affords a good prediction when based on the quality of the dispersed core.

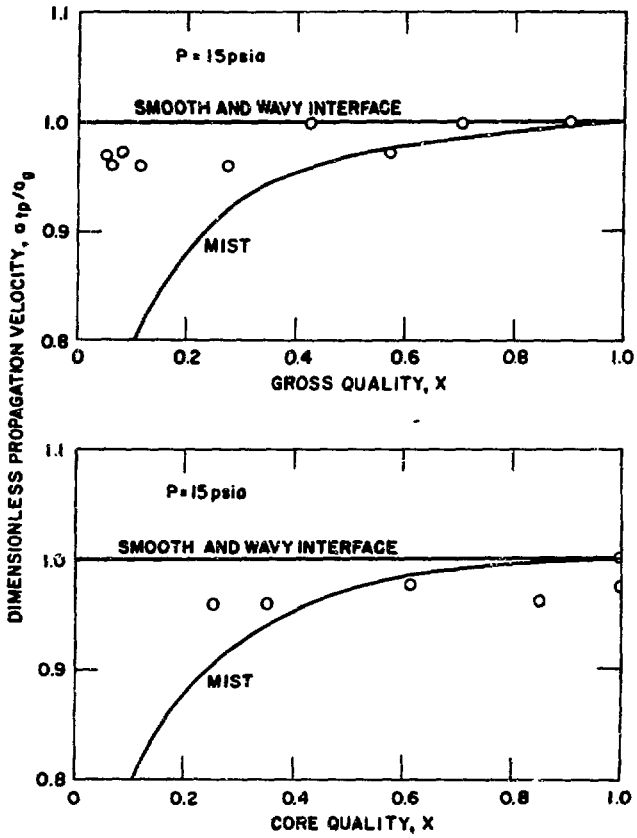

Fig. 32. Comparison of the One-component Models with the Rarefaction Wave Data of Collingham et al. as a Function of Gross and Core Qualities

In Figs. 30b, 31, and 32, the mist-flow velocities for rarefaction waves are slightly less than the analytical predictions. As was discussed above, the bulk wave behavior is preceded by a low-amplitude wave front which travels at the frozen velocity. The small interphase velocity differences set up behind this front could cause some viscous momentum transfer in the bulk behavior which would produce such lower velocities.

One final point to be mentioned is that, like the bubbly flows discussed above, the models and data discussed here are characteristic of small pulses traveling through a mixture which is initially in

equilibrium. Therefore, they are representative of neither sound waves nor critical flow, and should not be construed as "sonic" or "critical" velocities. As discussed above for bubbly mixtures and in Ref. 39 for droplet flows, the velocity of sound in two-phase media is frequency-dependent because of the relaxation times associated with the interphase transport of heat, mass, and momentum. It has also been shown in Refs. 20 and 40 that the velocities associated with one-component critical flows are characterized by considerable nonequilibrium in the mass-transfer process, and such flows cannot be treated by assuming negligible interphase mass transfer.

C. Comments on the Data of Semenov and Kosterin

Other than the annular-flow results of White and D'Arcy, the only one-component data reported for the void fraction range from 0.50 to 0.90 are the steam-water compression-wave results of Semenov and Kosterin.[12] In light of the other experimental studies enumerated above, this investigation requires special attention. The experimental results, which were obtained in vertical-up flow, are shown in Fig. 33. For comparison, the air-water data given in Ref. 12 for a horizontal channel are also shown. It is obvious that the air-water data do not agree with the results of Refs. 7, 9, and 17, which raises questions as to what flow pattern these unique data characterize. No flow-regime observations are given, but it is possible that some type of slug flow existed and the propagation

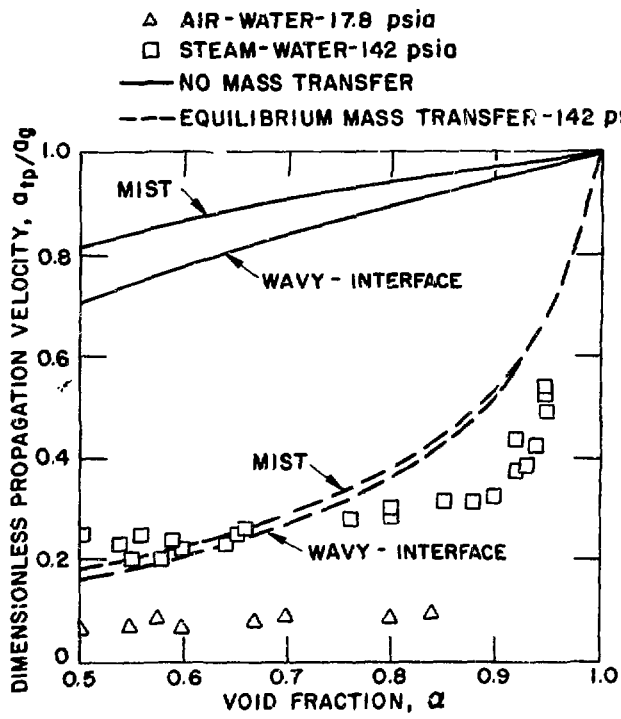

Fig. 33. One- and Two-component Experimental Results Reported by Semenov and Kosterin

was of the inertial type described in Ch. III and in Ref. 41. For most of the void-fraction range reported, this could also be true of one-component flows. However, for void fractions in the range from 0.90 to 1.0, a dispersed-annular configuration seems more likely than a slug pattern. Therefore, are the results characteristic of compression waves propagating through a one-component mist flow?

As was discussed in Ch. III, the vapor-controlled mass transfer for compression waves is generally so small that it can be neglected. However, Eq. 68 shows the bulk wave behavior is also dependent upon the ratio of the frozen and equilibrium velocities. In the void-fraction range investigated, this difference is quite large. Thus, perhaps the data of Ref. 12 satisfy Eq. 68 and, thus, are representative of the bulk of the wave traveling at the equilibrium velocity. The limiting mass-transfer curves are shown in Fig. 33 (only virtual-mass momentum transfer is considered), and the equilibrium mass-transfer solutions describe the general character of the data.

From the above discussion, it is apparent that a more definitive study of this regime is needed. Such a study should include not only rarefaction- and compression-wave data, but also detailed flow-regime observations.

D. Slug Flows

The results for the idealized slug flow are shown in Fig. 34. The measured velocity is in good agreement with the series propagation expression derived in Ch. III, which is to be expected. This idealized no-flow case illustrates the possible variation in propagation velocities for different flow regimes. The order-of-magnitude variations are dramatically demonstrated by the comparison of the bubbly, stratified, and slug-flow regimes as shown in Fig. 34.

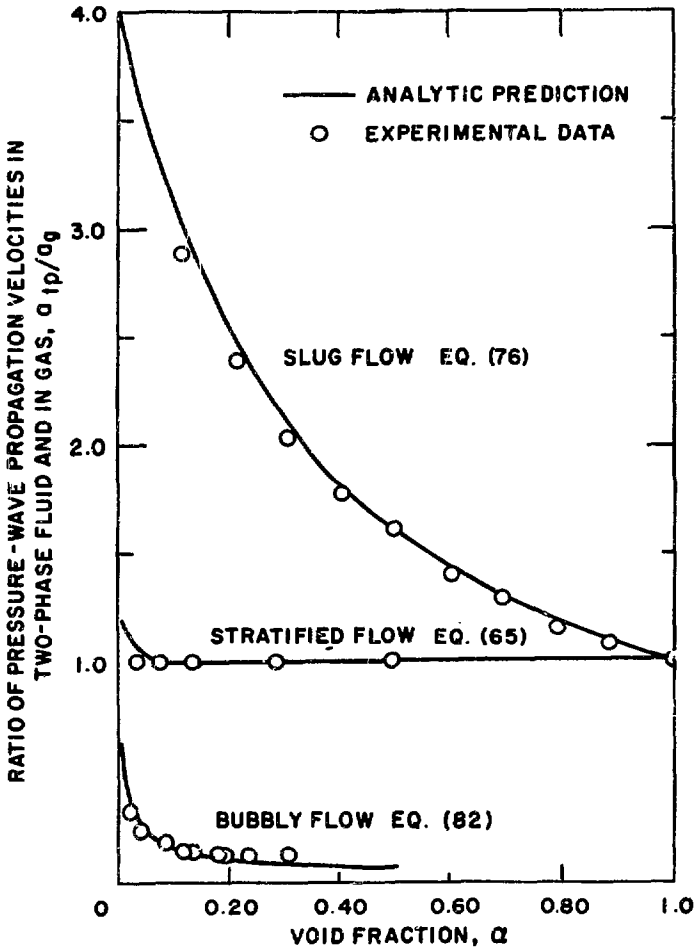

Fig. 34. Comparison of Propagation Velocities for Selected Flow Patterns

VI. SUMMARY AND CONCLUSIONS

The propagation velocities of small pressure pulses through one- and two-component two-phase mixtures were investigated experimentally and analytically. In the experimental program the frontal velocities of pressure waves in bubbly-like ($\alpha < 0.50$), stratified, and idealized slug flows were measured. Analytical models were developed for bubbly, mist, smooth separated, wavy separated, and slug-flow patterns. Interphase momentum transfer in bubbly, mist, and wavy separated flows is described by the virtual mass of the discrete phase. For smooth-interface separated-flow patterns, the rate of momentum transfer is assumed to be zero, and the results show that the propagation velocity is essentially equal to that of the gaseous phase. The slug-flow relationship is an idealized series-propagation solution which is only intended to illustrate one possible means of propagation in this flow pattern.

An analysis of the models and the experimental data leads to the following conclusions:

1. The most important conclusion is that the flow regime has an order-of-magnitude effect on the pressure-wave propagation velocities.

2. This strong dependency on flow regime is due to the large dependency of interphase momentum-transfer processes upon the flow pattern.

3. In bubbly-like flows ($\alpha < 0.50$), the rate of momentum transfer is quite large because of the virtual mass of the discrete gaseous phase.

4. Mist and wavy-interface configurations exhibit a small but noticeable rate of momentum transfer due to the virtual mass of the droplets and waves, respectively.

5. The smooth-interface separated flows exhibit a negligible rate of momentum transfer because neither phase exhibits any virtual-mass effects.

6. The low-quality, one-component frontal velocities and the time-pressure traces of the finite waves verify that the wave front propagates with no phase change in such flows.

7. The time-pressure traces show that the propagation velocities of compression and rarefaction waves are considerably different for portions of the wave removed from the frontal zone. This difference is a reflection of the different relaxation times associated with the mass-transfer

rates between two individually stable states and that between unstable conditions.

8. Analysis of the bulk wave velocity for mist flows indicates that rarefaction waves should propagate slower than compression pulses because of the larger mass-transfer rate in the former. This is borne out by the data.

9. The various models developed exhibit excellent agreement with the data characteristic of the respective flow regimes.

10. A comparison between the experimental propagation velocities of infinitesimal pulses and measurements of the velocity of sound show that, in two-phase flows, a clear distinction must be made between these two phenomena.

APPENDIX

Tabulated Data

The tabulated void fractions in the following tables are given to three significant figures for tabular consistency. The accuracy of the measurement of void fraction is a function of the steadiness of the flow and, thus, a function of the void fraction. Estimates of this dependency are given below.

VOID FRACTION	ACCURACY
0.000-0.050	±0.001
0.050-0.150	±0.010
0.150-0.300	±0.030
0.300-0.500	±0.050

Air-Water Data
(Bubble Flow)

Run	Pressure, psia	Temperature, °F	Void Fraction	Velocity, ft/sec
1000	25	80	0.040	257
1001	25	80	0.080	187
1002	25	80	0.085	183
1003	25	80	0.120	165
1004	25	80	0.150	155
1005	25	80	0.160	155
1006	25	80	0.005	570
1007	25	80	0.005	597
1008	25	80	0.009	458
1009	25	80	0.020	321
1010	25	80	0.035	270
1011	25	80	0.070	205
1012	25	80	0.020	347
1013	25	80	0.040	257
1014	25	80	0.090	197
1015	25	80	0.120	165
1016	25	80	0.140	160
1017	25	80	0.170	155
1018	25	80	0.180	151
1019	25	80	0.200	147
1020	25	80	0.240	147
1021	25	80	0.310	147
1022	25	80	0.070	174
1023	25	80	0.140	160
1024	25	80	0.160	155
1025	25	80	0.210	142
1026	25	80	0.260	139
1027	25	80	0.330	137
1028	25	80	0.330	133
1029	25	80	0.330	139
1030	25	80	0.380	139
1031	25	80	0.380	149
1032	25	80	0.380	155
1033	25	80	0.380	139
1034	25	80	0.380	147
1035	25	80	0.380	147
1036	25	80	0.380	147
1037	25	80	0.380	151
1038	25	80	0.430	151
1039	25	80	0.430	155

Run	Pressure, psia	Temperature, °F	Void Fraction	Velocity, ft/sec
1040	25	80	0.430	171
1041	25	80	0.200	143
1042	25	80	0.190	141
1043	25	80	0.390	151
1044	25	80	0.390	149
1045	25	80	0.400	158
1100	35	80	0.016	493
1101	35	80	0.030	366
1102	35	80	0.080	233
1103	35	80	0.150	183
1104	35	80	0.010	493
1105	35	80	0.019	414
1106	35	80	0.031	338
1107	35	80	0.040	277
1108	35	80	0.050	250
1109	35	80	0.070	233
1110	35	80	0.090	218
1111	35	80	0.110	201
1112	35	80	0.120	190
1113	35	80	0.130	187
1114	35	80	0.140	190
1115	35	80	0.160	180
1200	45	80	0.006	658
1201	45	80	0.033	347
1202	45	80	0.018	428
1203	45	80	0.053	293
1204	45	80	0.070	257
1205	45	80	0.020	414
1206	45	80	0.040	321
1207	45	80	0.065	270
1208	45	80	0.070	257
1209	45	80	0.090	244
1210	45	80	0.100	239
1211	45	80	0.120	223
1212	45	80	0.130	218
1213	45	80	0.140	201
1214	45	80	0.160	201
1215	45	80	0.180	197
1216	45	80	0.002	1221
1217	45	80	0.005	965

Run	Pressure, psia	Temperature, °F	Void Fraction	Velocity, ft/sec
1218	45	80	0.014	570
1219	45	80	0.010	641
1300	55	80	0.005	733
1301	55	80	0.011	611
1302	55	80	0.014	570
1303	55	80	0.027	435
1304	55	80	0.038	366
1305	55	80	0.050	329
1306	55	80	0.060	311
1307	55	80	0.072	293
1308	55	80	0.085	270
1309	55	80	0.095	257
1310	55	80	0.003	855
1311	55	80	0.008	733
1312	55	80	0.020	513
1313	55	80	0.030	414
1314	55	80	0.042	356
1315	55	80	0.055	321
1316	55	80	0.070	285
1317	55	80	0.085	263
1318	55	80	0.102	244
1400	65	80	0.005	916
1401	65	80	0.011	693
1402	65	80	0.015	641
1403	65	80	0.022	513
1404	65	80	0.030	435
1405	65	80	0.040	401
1406	65	80	0.052	366
1407	65	80	0.065	321
1408	65	80	0.075	302
1409	65	80	0.090	293
1410	65	80	0.095	277
1411	65	80	0.105	277
1412	65	80	0.115	270
1413	65	80	0.127	257
1414	65	80	0.138	250
1415	65	80	0.150	250
1416	65	80	0.160	244
1417	65	80	0.170	239
1418	65	80	0.190	233
1419	65	80	0.210	228
1420	65	80	0.210	228

Air-Water Data
(Stratified)

Run	Pressure, psia	Temperature, °F	Void Fraction	Velocity, ft/sec
1500	25.0	80.0	1.000	1166
1501	25.0	80.0	0.500	1166
1502	25.0	80.0	0.500	1140
1503	25.0	80.0	0.290	1166
1504	25.0	80.0	0.140	1166
1505	25.0	80.0	0.080	1140
1506	25.0	80.0	0.035	1166

Air-Water Data
(Slug Flow)

Run	Pressure, psia	Temperature, °F	Void Fraction	Velocity, ft/sec
1600	25.0	70.0	1.000	1125
1601	25.0	70.0	0.885	1235
1602	25.0	70.0	0.795	1315
1603	25.0	70.0	0.695	1470
1604	25.0	70.0	0.608	1580
1605	25.0	70.0	0.502	1810
1606	25.0	70.0	0.409	2030
1607	25.0	70.0	0.308	2300
1608	25.0	70.0	0.220	2740
1609	25.0	70.0	0.124	3270
1610	25.0	70.0	0.000	4600

Steam Water Data
Bubble-flow Equilibrium Mixture

Run	Pressure, psia	Vapor Void Fraction	Propagation Velocity, ft/sec	Pulse[a]
1700	36	0.011	564	C
1701	36	0.013	518	R
1702	35	0.013	466	R
1703	36	0.014	583	R
1704	36	0.014	475	C
1705	36	0.015	513	R
1706	36	0.015	500	C
1707	42	0.025	352	R
1708	42	0.025	289	R
1709	42	0.025	332	R
1710	42	0.026	331	C
1711	41	0.027	309	C
1712	43	0.032	354	R
1713	43	0.034	350	R
1714	45	0.050	320	C
1715	45	0.050	336	R
1716	41	0.050	306	R
1717	46	0.052	277	R
1718	40	0.056	231	C
1719	40	0.059	257	R
1720	41	0.060	306	C
1721	40	0.081	231	R
1722	45	0.083	225	R
1723	40	0.086	205	R
1724	40	0.086	267	C
1725	40	0.086	205	R
1726	41	0.091	225	C
1727	45	0.091	219	C
1728	41	0.092	190	R
1729	39	0.096	241	C
1730	47	0.098	235	C
1731	46	0.103	214	C
1732	46	0.104	249	R
1733	40	0.108	233	R
1734	46	0.110	217	R
1735	40	0.117	176	C

[a] R - Rarefaction Pulse; C - Compression Pulse

Run	Pressure, psia	Vapor Void Fraction	Propagation Velocity, ft/sec	Pulse
1736	41	0.123	196	C
1737	41	0.123	209	C
1738	38	0.125	244	C
1739	39	0.128	223	R
1740	46	0.136	256	C
1741	39	0.139	247	R
1742	39	0.140	196	R
1743	39	0.156	177	C
1744	39	0.158	205	R
1745	41	0.161	221	C
1746	41	0.165	180	C
1747	39	0.168	170	R
1748	41	0.169	192	R
1749	41	0.170	197	R
1750	39	0.171	167	R
1751	39	0.173	151	C
1752	39	0.173	182	R
1753	41	0.177	210	C
1754	39	0.187	174	R
1755	41	0.189	180	R
1756	42	0.191	208	C
1757	41	0.195	174	R
1758	43	0.197	212	C
1759	40	0.197	139	C
1760	41	0.203	171	C
1761	41	0.212	190	C
1762	41	0.215	180	R
1763	42	0.218	233	C
1764	39	0.222	169	R
1765	42	0.224	203	R
1766	41	0.224	221	R
1767	42	0.225	171	C
1768	40	0.227	174	R
1769	41	0.227	197	C
1770	41	0.127	190	C
1771	41	0.294	214	C
1772	41	0.299	206	C
1773	41	0.299	218	C
1774	41	0.315	236	C
1775	41	0.321	196	C
1776	41	0.321	233	C

Steam Water Data
Stratified Media (Equilibrium)

Run	Pressure, psia	Vapor Volume Fraction	Propagation Velocity, ft/sec	Pulse[a]
1800	14.7 ± 0.2	0.130	1525	C
1801	"	0.155	1480	R
1802	"	0.275	1500	R
1803[b]	"	0.275	1525	C
1804[b]	"	0.500	1545	C
1805[b]	"	0.500	1480	R
1806	"	0.505	1500	R
1807	"	0.495	1525	C
1808	"	0.625	1500	R
1809	"	0.640	1550	C
1810[b]	"	0.750	1550	C
1811[b]	"	0.750	1500	R
1812	"	0.855	1500	R
1813	"	0.855	1525	C
1814	"	1.0	1525	C
1900	50 ± 1	0.400	1550	R
1901	"	0.400	1575	C
1902	"	0.565	1575	R
1903	"	0.565	1575	C
1904	"	0.650	1600	R
1905	"	0.650	1600	C
1906	"	0.900	1575	R
1907	"	0.900	1600	C
1908	"	1.0	1575	R
1909	"	1.0	1600	C

[a] R - Rarefaction Pulse
C - Compression Pulse

[b] These runs were repeated several times with transducers located both in the vapor phase and in the liquid phase.

ACKNOWLEDGMENTS

During the construction and operation of the experimental facility the technical assistance of Messrs. Daniel Quinn, William Jeans, Elmer Gunchin, and George Lambert proved invaluable and is gratefully acknowledged.

REFERENCES

1. H. K. Fauske, *Two-Phase Compressibility Phenomena and How They Effect Reactor Safety*, Power Reactor Technology and Reactor Fuel Processing, *10*, No. 1 (Winter 1966-67).

2. H. K. Fauske, "Propagation of Pressure Disturbances in Two-Phase Flow," *Proc. Symp. Two-Phase Flow Dynamics, Eindhoven, Netherlands*, Sept. 4-9, 1967.

3. G. Grass, H. Kottowski, and R. Warnsing, *Das Sieden von Flussigen Alkalimetallen*, Atomkernenergie, *12*, Heft 304 (1967).

4. E. G. Schlechtendahl, *Die Ejektion von Natrium aus Reaktor kuhlkanalen*, Nukleonik, *10*, Heft 5 (1967).

5. *Reactor Development Program Progress Report for March 1969*, ANL-7561, pp. 93-94.

6. H. K. Fauske, "Liquid Metal Boiling in Relation to LMFBR Safety Design," *Proc. AIChE-ASME 10th National Heat Transfer Conference*, Philadelphia, Pa. (1968).

7. R. G. Evans, S. W. Gouse, and A. E. Bergles, *Pressure Wave Propagation in Adiabatic Two-Phase Flow*, MIT Report No. DSR 74629-2.

8. S. W. Gouse, Jr. and R. G. Evans, "Acoustic Velocity in Two-Phase Flow," *MIT Notes Special Summer Session in Two-Phase Flow and Heat Transfer* (1967).

9. L. J. Hamilton, *Propagation of Pressure Waves in Two-Phase Media*, Ph.D. Thesis, University of California, Berkeley, Calif. (Sept. 1968).

10. I. J. Campbell and A. S. Pitcher, *Shock Waves in a Liquid Containing Gas Bubbles*, Proc. Roy. Soc. (London), A243, 534-545, 1235 (1958).

11. H. B. Karplus, *Propagation of Pressure Waves in a Mixture of Water and Steam*, ARF 4132-12 (Jan. 1961).

12. N. I. Semenov and S. I. Kosterin, *Results of Studying the Speed of Sound in Moving Gas-Liquid Systems*, Teploenergetika, *11* (6), 46-51 (1964).

13. F. V. D. Walle, A. J. Verheugen, V. J. M. Haagh, and M. Bogaardt, *A Study of the Application of Acoustical Methods for Determining Void Fraction in Boiling Water Systems*, EUR, 2336, e. (June 1965).

14. V. J. DeJong and J. C. Firey, *Effect of Slip and Phase Change on Sound Velocity in Steam-Water Mixtures and the Relation to Critical Flow*, I&EC Process Design and Development, *7* (3) (July 1968).

15. R. E. Collingham and J. C. Firey, *Velocity of Sound Measurements in Wet Steam*, I&EC Process Design and Development, *2* (3), 197-202 (1963).

16. W. G. England, J. C. Firey, and O. E. Trapp, *Additional Velocity of Sound Measurements in Wet Steam*, I&EC Process Design and Development, *5* (2), 198-202 (1966).

17. C. W. Garrard, Jr., *A Study of the Propagation of Small Amplitude Pressure Pulses in a Two-Phase, Two-Component Mixture with an Annular Flow Pattern*, Ph.D. Thesis, Nuclear Engineering Dept., Texas A&M University (1968).

18. R. F. White and D. F. D'Arcy, "Velocity of Sound and Critical Discharge Pressure in Annular Two-Phase Flow," Paper No. 5 presented at *Symp. of Fluid Mechanics and Measurements in Two-Phase Flow Systems*, Univ. of Leeds, England (1969).

19. R. F. Tangren, C. H. Dodge, and H. S. Seifert, *Compressibility Effects in Two-Phase Flow*, J. Appl. Phys., *20* (7), 637-645 (1949).

20. R. E. Henry, *A Study of One- and Two-component Two-phase Critical Flows at Low Qualities*, ANL-7430 (March 1968).

21. A. L. Davies, *The Speed of Sound in Mixtures of Water and Steam*, AEEW-M452 (1956).

22. J. M. Clinch and H. B. Karplus, *An Analytical Study of the Propagation of Pressure Waves in Liquid Hydrogen-Vapor Mixtures*, NASA CR-54015 (May 1964).

23. J. E. Hench and J. P. Johnston, *Two-Dimensional Diffuser Performance with Subsonic, Two-Phase, Air-Water Flow*, APED-5477 (Jan. 1968).

24. V. L. Streeter, *Fluid Mechanics*, 2nd Edition, McGraw Hill Book Co., Inc., New York (1958).

25. J. H. Linehan, *The Interaction of Two-dimensional, Stratified, Turbulent Air-Water and Steam-Water Flows*, ANL-7444 (May 1968).

26. L. M. Milne-Thompson, *Theoretical Hydrodynamics*, 4th Edition, The Macmillan Co., New York (1960).

27. J. Roseman and V. Agosta, "Propagation of Sound in a Reacting Gas Mixture Near Equilibrium," *The Performance of High Temperature Systems*, 2, Edited by Gilbert S. Bahn, Gordon and Breach, New York (1969).

28. R. W. Springer and S. Gratch, *The Speed of Sound in a Chemically Reacting Gas*, ASME Paper No. 67-FE02 presented at the Fluids Engineering Conference, Chicago, May 8-11, 1967.

29. P. P. Wegener, and J. D. Cole, "Experiments on Propagation of Weak Disturbances in Stationary Supersonic Nozzle Flow of Chemically Reacting Gas Mixtures," *Eighth Symposium on Combustion*, The Williams and Wilkins Co., Baltimore (1962) p. 348.

30. P. G. Hill, *Condensation of Water Vapour During Supersonic Expansion in Nozzles*, J. Fluid Mech., *25*, 593 (1966).

31. T. F. Hueter and R. H. Bolt, *Sonics*, John Wiley and Sons, New York (1955) pp.38-39.

32. J. H. Keenan and F. G. Keyes, *Thermodynamic Properties of Steam*, 1st Edition, John Wiley and Sons, Inc., New York (1959).

33. T. Kobori, S. Yokoyama, and H. Miyashiro, *Propagation Velocity of Pressure Waves in Pipe Lines*, Hitachi Hyoron, *37* (1955).

34. B. R. Parkin, F. R. Gilmore, and H. L. Brode, *Shock Waves in Bubbly Wave*, Rand Corp. RM-2795-PR (1961).

35. H. B. Karplus, *The Velocity of Sound in a Liquid Containing Gas Bubbles*, IIT Report COO-248 (1958).

36. G. F. Hewitt, *Photographic and Entrainment Studies in Two-phase Flow Systems*, AERE-R4683 (1964).

37. R. W. Lockhart and R. C. Martinelli, *Proposed Correlation of Data for Isothermal Two-phase, Two-component Flow in Pipes*, Chem. Eng. Progress, *45*, 39 (1949).

38. J. G. Collier, *Heat Transfer and Fluid Dynamic Research as Applied to Fog Cooled Power Reactors*, AECL-1631 (1962).

39. M. E. Deich, G. A. Filippov, E. V. Stekol'shckikov, and M. P. Anisimove, *Experimental Study of the Velocity of Sound in Wet Steam*, Thermal Engineering, *14*, 59 (1967).

40. R. E. Henry, *Discussion of "A Pressure Pulse Model for Two-Phase Critical Flow and Sonic Velocity,"* Trans. ASME, *91-C*, 382 (1969).

41. R. E. Bowles and F. M. Manion, *Analysis and Test of Signal Transmission in a Multiphase Fluid Mixture*, U. S. Army Aviation Material Laboratories, Report 65-77 (1966). (AD628676)